



# Removal of reactive black 5 in water using adsorption and electrochemical oxidation technology: kinetics, isotherms and mechanisms

V. Ganthavee<sup>1</sup> · A. P. Trzcinski<sup>1</sup>

Received: 15 July 2023 / Revised: 12 April 2024 / Accepted: 25 April 2024 / Published online: 21 May 2024  
© The Author(s) 2024

## Abstract

In this work, a novel graphite intercalation compound (GIC) particle electrode was used to investigate the adsorption of Reactive Black 5 (RB5) and the electrochemical regeneration in a three-dimensional (3D) electrochemical reactor to recover its adsorptive capacity. Various adsorption kinetics and isotherm models were used to characterise the adsorption behaviour of GIC. Several adsorption kinetics were modelled using linearised and non-linearised rate laws to evaluate the viability of the sorption process. Studies on the selective removal of RB5 dyes from binary mixture in solution were evaluated. RSM optimisation studies were integrated with ANOVA analysis to provide insight into the significance of selectivity reversal from the salting effect of textile dye solution on GIC adsorbent. A unique range of adsorption kinetics and isotherms were used to evaluate the adsorption process. Non-linear models best simulated the kinetic data in the order: Elovich > Bangham > Pseudo-second-order > Pseudo-first-order. The Redlich–Peterson isotherm was calculated to have a dye loading capacity of 0.7316 mg/g by non-linear regression analysis. An error function analysis with ERRSQ/SSE of 0.1390 confirmed the accuracy of dye loading capacity predicted by Redlich–Peterson isotherm using non-linear regression analysis. The results showed that Redlich–Peterson and SIPS isotherm models yielded better fitness to experimental data than the Langmuir type. The best dye removal efficiency achieved was ~93% using a current density of 45.14 mA/cm<sup>2</sup>, whereas the highest TOC removal efficiency achieved was 67%.

**Keywords** Dye · Adsorption · Electrochemical oxidation · Graphite intercalation compound · Kinetics · Isotherms

## Introduction

Organic contaminants such as dyes and pigments are recalcitrant pollutants highly resistant to environmental biodegradation. These pollutants are often discharged into water from industrial effluents such as dye and paint manufacturing, food processing, textile, etc. Most of these dyes are synthetic, which means they can be highly toxic and carcinogenic if it finds its way into the food chain. Therefore, there is an urgent need to remove the dyes from liquid waste until they fall below a specific concentration acceptable to

environmental regulatory authorities. There are several ways to remove dyes from water, such as adsorption (El-Kammah et al. 2022; Noorimotlagh et al. 2019), membrane filtration (Ma et al. 2022; Mansor et al. 2020), chemical coagulation and flocculation (Lau et al. 2014; Szyguła et al. 2009), photocatalytic degradation (Fernandes et al. 2019; Tekin 2014), electrocoagulation/electroflotation (Balla et al. 2010), Fenton process (Suhan et al. 2021), electrochemical oxidation (Kumar and Gupta 2022; Song et al. 2010) etc. Adsorption is an attractive and effective approach to removing contaminants from water, particularly when the adsorbent is cheap, has minimal sludge generation and does not require an additional pre-treatment process (Sultana et al. 2022). The adsorption method is simple and cost-effective, and high dye removal efficiency can be achieved (Chaiwichian and Lunphut 2021). Several attempts have been made to electrochemically regenerate activated carbon adsorbents (Narbaitz and McEwen 2012; Xing et al. 2023). However, low electrical conductivity of liquid media limited the energy

---

Editorial responsibility: Samareh Mirkia.

---

✉ V. Ganthavee  
Voravich.Ganthavee@usq.edu.au

<sup>1</sup> School of Agriculture and Environmental Science, University of Southern Queensland, 487-535 West St, Darling Heights, Toowoomba, QLD 4350, Australia



required to regenerate activated carbon adsorbents (Karimi-Jashni and Narbaitz 2005). Activated carbon adsorbents have a high degree of porosity, which affects its ability to regenerate successfully. Offsite thermal regeneration is required for activated carbon. However, exhausted activated carbon is often disposed into a landfill or incinerated, which may contribute to secondary pollution. Hence, graphite intercalation compound (GIC) can be used as an alternative to removing dissolved organic contaminants from water. GIC can be electrochemically regenerated in situ by an electrochemical oxidation process. It is electrically conductive and requires a short adsorption time to reach equilibrium (Mohammed et al. 2012). However, the specific surface area of GIC is significantly smaller than activated carbon.

Previous studies have shown that the combined adsorption and electrochemical regeneration of GIC can maximise dye removal efficiency (Hussain et al. 2015b; Mohammed et al. 2012). Optimising operating conditions allows the formation of chlorinated breakdown products to be minimised during electrochemical regeneration to prevent side reactions (Hussain et al. 2015a). However, there is a lack of studies focusing on the adsorption models used to model GIC using statistical analysis and comparison of linear and non-linear regression models to describe the adsorption mechanisms of GIC. In this paper, we report the kinetics and isotherm studies used to examine the adsorption behaviour of GIC. In addition, the effect of current density in the subsequent electrochemical oxidation process was also investigated to optimise the dye and TOC removal efficiencies.

## Materials and methods

### Adsorbate

Reactive Black 5 (RB5) dye, with an empirical formula of  $C_{26}H_{21}N_5Na_4O_{19}S_6$  was purchased from Sigma-Aldrich with the product number 306452. The chemical structure of the Reactive Black 5 dye is shown below. A stock solution of 100 mg/L was prepared from the dissolution of RB5 in water.

### Adsorbent preparation

The adsorbent used in this study is an expandable graphite intercalation compound (GIC) purchased from Sigma-Aldrich (P/N: 808121). At least 75% of the flakes were larger than 300 microns (See Supplementary Material S1). GIC has no porous structure and a relatively low electroactive surface area of approximately  $1 \text{ m}^2/\text{g}$  (Hussain et al. 2016). It is highly conductive, with  $0.8 \text{ S/cm}$  (Asghar et al. 2014).

### Determination of pH point of zero charge ( $\text{pH}_{\text{pzc}}$ )

The point of zero charge (pzc) of the GIC adsorbent was determined using a pH meter (Eutech instruments, PC 2700). A mixture of 50 mg GIC in 40 mL of distilled water containing 0.1 M HCl and 0.1 M NaOH to adjust the pH levels ranging between 3 and 12. The pH was measured after 24 h of equilibration at an ambient temperature of  $22.5 \text{ }^\circ\text{C}$ . The  $\text{pH}_{\text{pzc}}$  is defined as the pH at which the surface charge of the GIC adsorbent is neutral.

### Adsorption studies

The adsorption kinetic studies were performed to determine the adsorption system's reaction order and identify the rate-limiting process. The adsorption studies were performed for Reactive Black 5 dye at various initial concentrations using a GIC adsorbent dosage of 23 g/L, which was within the ratios of adsorbent concentration estimated across different works of literature such as Hussain et al. (2015b), Liu et al. (2016) and Purkait et al. (2007). The mechanical agitation speed was adjusted to 300–400 rpm at  $22 \text{ }^\circ\text{C}$ . The adsorption time was between 0 and 120 min until the adsorption equilibrium for various initial dye concentrations was reached. In order to investigate the effect of salt on the selectivity of GIC, adsorption experiments were carried out using sodium chloride ( $\text{NaCl}$ ,  $\geq 99\%$ , Sigma-Aldrich, Australia) at concentration ranging from 1 to 10 g/L. The adsorbent loading,  $q_t$  (mg/g), is to be determined from the initial and final concentrations at specific time intervals as given in Eq. (1):

$$q_t = \frac{(C_i - C_f)}{m} V \quad (1)$$

where  $C_i$  and  $C_f$  are the initial and final concentrations (mg/L) of Reactive Black 5 solution,  $V$  is the volume (L) of a solution, and  $m$  is the mass (g) of the adsorbent used. Microsoft Excel Solver Add-In (2022) was used to perform graphical plots, curve fitting and mathematical models for adsorption kinetics and isotherms by comparing the experimental and theoretical data. The chi-square test is a critically important error function in determining the best fit of isotherm model applicable to the tested adsorption system. It estimates the difference in squares between the theoretical data based on the predicted model and the experimental data collected and then divides each difference by the corresponding experimental value.

The influence of the variables was examined at three different levels, and the values of the variables at each level are shown in Table 1. The total number of experimental runs was designed using the CCD method by Eq. (2):

**Table 1** Range and codification of the independent variable ( $x_i$ ) were used in the experimental design

Independent variables	Symbol	$-\alpha$	$-1$	$0$	$+1$	$+\alpha$
Temperature, ( $^{\circ}\text{C}$ )	$X_1$	30	36.0809	45	53.9191	60
pH	$X_2$	3	4.6216	7	9.3784	11
Salt concentration (g/L)	$X_3$	1	2.8243	5.5	8.1757	10

$$n = 2^i + 2i + n_0 \quad (2)$$

where  $n$  is the total number of experimental runs,  $i$  is the number of independent variables, and  $n_0$  is the number of centre points. A total of 20 experiments were designed. A quadratic polynomial equation can be used to mathematically express the relationship between the independent variables and the responses, as shown in Eq. (3):

$$Y = \beta_0 + \sum_{i=1}^k \beta_i x_i + \sum_{i=1}^k \beta_{ii} x_i^2 + \sum_{i=1}^{k-1} \sum_{j=i+1}^k \beta_{ij} x_i x_j + \gamma \quad (3)$$

where  $Y$  is the predicted response,  $\beta_0$  is the constant term,  $\beta_0$ ,  $\beta_{ij}$  and  $\beta_{ii}$  are the linear, second-order and interaction coefficients, respectively,  $x_i$  and  $x_j$  are the independent variables, and  $x_i x_j$  represents the first-order interaction between  $x_i$  and  $x_j$ ,  $k$  is the number of independent variables, and  $\gamma$  is a random error.

### Adsorption and electrochemical regeneration

Electrochemical regeneration of GIC adsorbent was carried out in a batch electrochemical cell, as shown in Fig. 1.

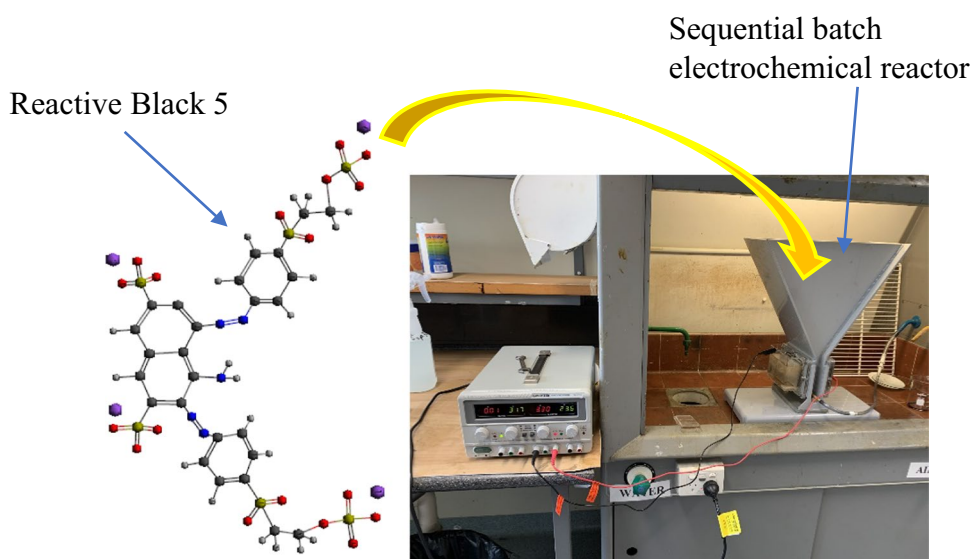
Direct anodic oxidation of dye pollutants occurs via graphite anode, whereas indirect oxidation occurs via electrogenerated highly reactive oxidising species such as hydroxyl radicals and active chlorine species. The

adsorption-electrochemical treatment process consists of three essential steps: initial adsorption-regeneration and re-adsorption via electrochemical treatment (Hussain et al. 2015b). In this experiment, 2,000 mL of the 100 mg/L of RB5 stock solution was subjected to electrochemical treatment. The dye solution was poured into a sequential batch reactor, and adsorption occurred when the air compressor was switched on. The air was sparged into the bottom of the chamber to facilitate mixing between GIC and dye solution. The active area of each electrode used in the reactor was 70 cm<sup>2</sup>. The interelectrode distance between the anode and cathode was 6.3 cm, and about 200 g of GIC was added to fill the regeneration zone (12 cm deep and 5 cm thick) before pouring the dye solution. The volume of the reactor chamber was about 6–7 L. A 30 V DC power supply unit was connected to the graphite anode and 316-grade stainless steel cathode to facilitate an electrochemical redox reaction. The cathodic compartment was filled with 0.3% (w/v) acidified brine solution pH of 1–2 separated from the dye solution by a Daramic membrane (Daramic, USA). The current supply ranged from 0.21 to 3.16 A, corresponding to a current density of 3 to 45.14 mA/cm<sup>2</sup>.

### Analytical methods

Surface characterisation of GIC can be performed using IRAffinity-1S, GladiaATR 10 Shimadzu Fourier Transform

**Fig. 1** RB5 textile dye wastewater in the sequential batch electrochemical reactor



Infrared Spectroscopy (FTIR) by examining its surface functional group or surface chemistry. Scanning Electron Microscopy (SEM) is used to investigate the surface morphology or textural properties of the GIC. A detailed analysis of GIC characteristics using FTIR and SEM is shown in Supplementary Material.

UV/Visible spectrophotometer (DR6000, Hach) determined the RB5 dye concentrations in solution at different time intervals. The maximum absorption occurred at a wavelength  $\lambda = 596$  nm as specified by previous authors Feng et al. (2022), Saroyan et al. (2019) and Droguett et al. (2020). TOC-V CSH Shimadzu TOC analyser is used to determine the degree of mineralisation of the Reactive Black 5 dye before and after the electrochemical treatment. A Hach DR6000 UV/Visible Spectrophotometer was used to determine the RB5 concentrations in the samples. The Coefficient of Variation (de Fouchécour et al. 2022) for UV-absorbance analysis of RB5 is approximately 0.31%, whereas for TOC analysis is approximately 1.69%.

## Results and discussion

### Adsorption studies

The adsorption kinetics pertain to the uptake rate of RB5 adsorbates by GIC. Figure 2a shows the dye removal efficiency for various initial dye concentrations ranging from 33.81 to 136.67 mg/L. The dye removal efficiencies for different initial dye concentrations fluctuated throughout the adsorption period. This adsorption phenomenon indicated that the dye molecules adsorbed onto the GIC adsorbent and desorbed from the adsorbent surface back and forth due to weak intermolecular interaction. Dye sorption usually occurs when the dye molecules are diffused from the bulk liquid onto the adsorbent surface through the solid–liquid interface between the adsorbent surface and the bulk solution. The dye molecules interact with the active sites on the surface of the adsorbent through intermolecular interactions, which are held by either van der Waals' forces, electrostatic interactions, hydrophobic interactions,  $\pi$ – $\pi$  electron donor–acceptor interactions, hydrogen bonding etc. The binding process is reversible if the solute–substrate interaction is held by weak intermolecular forces such as van der Waals' forces. The binding process is irreversible if there is a strong electrostatic attraction between the solute and substrate. In addition, Fig. 2a shows the dye removal efficiencies for various initial dye concentrations. It was found that the higher the initial dye concentration, the lower the overall dye removal efficiency due to the limited availability of active sites and rapid uptake of adsorbates onto active sites.

Figure 2b indicates that adsorbent loading increased within the first 0–8 min for initial RB5 dye concentrations ranging from 33.81 to 136.67 mg/L, eventually reaching an adsorption equilibrium. However, continuous adsorption–desorption occurred throughout the experimental conditions even after 100 min of adsorption time. The rise and fall of adsorbent loadings strongly indicated that the dye molecules continuously adsorbed and desorbed from the surface of the GIC adsorbent due to weak intermolecular interactions. This indicated the reversibility of the solute–substrate binding process.

On the other hand, pseudo-second-order kinetic models showed an excellent curve fitting between experimental and theoretical data (Fig. 3a), indicating that it is suitable to describe the adsorption–desorption kinetics in experimental studies. Non-linearised pseudo-first-order kinetic models yield better fitness than the linearised pseudo-second-order kinetic model (Table 1). The desorption process increased dye concentration in the bulk liquid, creating a greater concentration gradient and a greater diffusion flux of dye adsorbates re-adsorbing onto the GIC adsorbent surface. Although the adsorption kinetics of RB5 exhibited a slow rate-limiting step, the high concentration gradient improved the surface diffusivity or diffusion flux of the dye adsorbates onto the GIC adsorbent surface, reaching a rapid equilibrium point within 3 min of adsorption time.

The Bangham model is derived from the generalisation of the Weber and Morris model (Largitte and Pasquier 2016; Sumanjit et al. 2016). The kinetic data obtained from this model can be used to determine the slow limiting step in the adsorption system, as shown in Table 1. The equation indicates that  $q$  denotes the dye loading per mass of adsorbent (mg/g),  $\theta$  and  $k$  represent kinetic constants. This kinetic model can be used to verify whether the rate-limiting step influences the pore or surface diffusion.

Furthermore, a novel three-stage kinetic model was used to describe the adsorption of RB5 onto GIC adsorbent. The model is based on the concept of mass conservation for RB5 combined with three distinct stages of adsorption onto GIC (Choi et al. 2007): 1) the first portion of the plot represents an instantaneous stage or external surface adsorption; 2) the second portion of the gradual stage in the plot represents the rate-limiting intraparticle diffusion; and 3) the third portion for a constant stage represents the aqueous phase which no longer interacts with GIC. The analytical three-stage kinetic model can be validated with the kinetic data from the batch experimental study involving RB5 adsorption onto the GIC.

The significance of developing a three-stage kinetic model for each initial dye concentration through modelling studies stems from strong evidence that different stages of adsorption exist in the kinetic models. The first stage involves a sharper portion of the adsorption curvature, representing the rapid decrease in the aqueous phase concentration. Dye

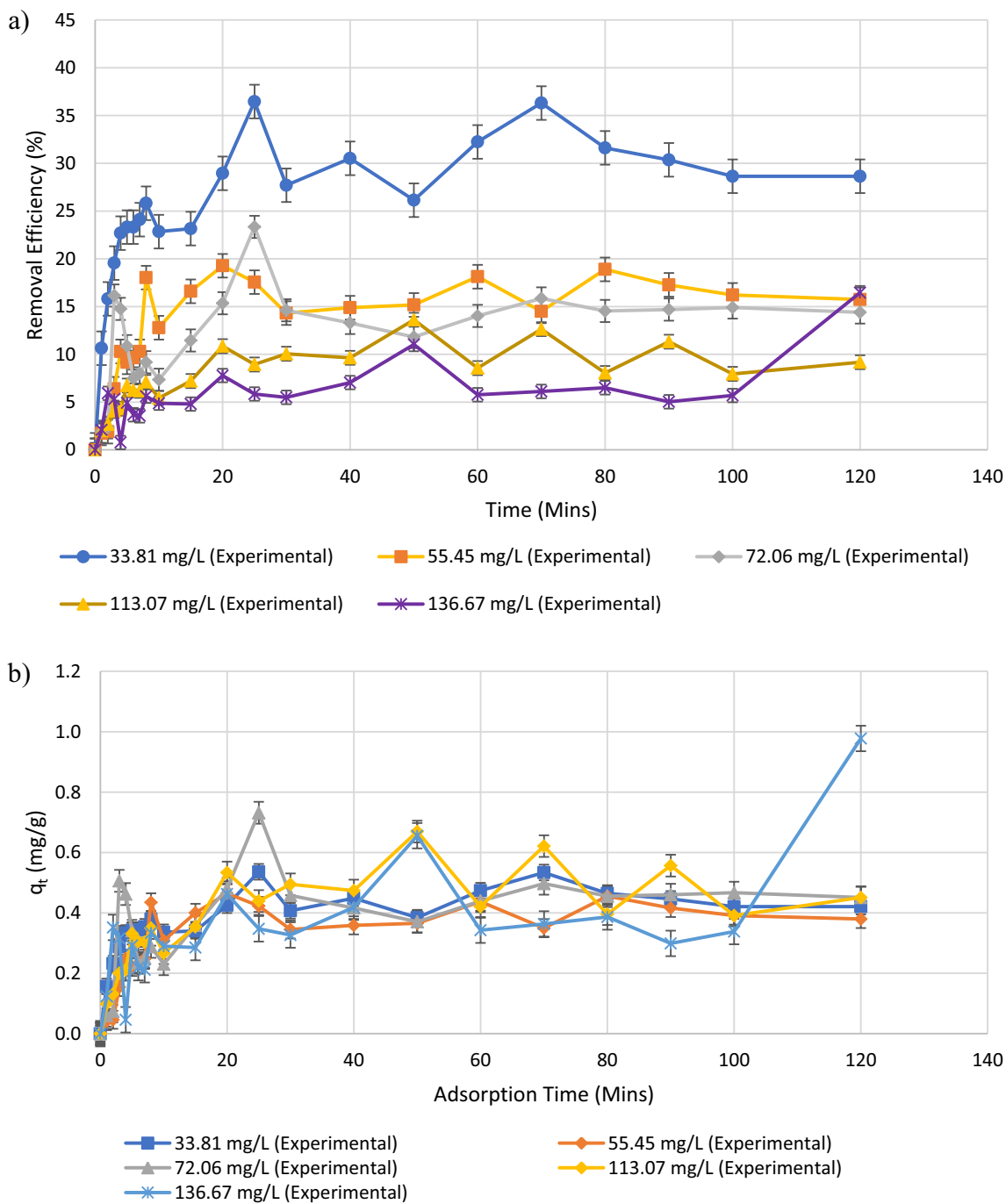


**Fig. 2** a The changes in dye removal efficiencies over a period of time for various initial dye concentrations; b the adsorbent loading of Reactive Black 5 dye onto GIC over adsorption time from 0 to 120 min

molecules diffuse into the bulk solution, moving across the solid–liquid interface and binding to the active sites on the external surface of the adsorbent by instantaneous adsorption. The second gradual decline portion represents the slow rate-limiting adsorption influenced by intraparticle or surface diffusion. In contrast, the third constant line portion represents a minimal change in aqueous phase concentration or

indicates equilibrium has been reached. Compared to standard kinetic expressions, pseudo-second-order equation, and Elovich kinetic equation, these three-stage kinetic models are purely empirical. They do not discriminate between the different adsorption stages, such as instantaneous versus rate-limiting adsorption (Choi et al. 2007).

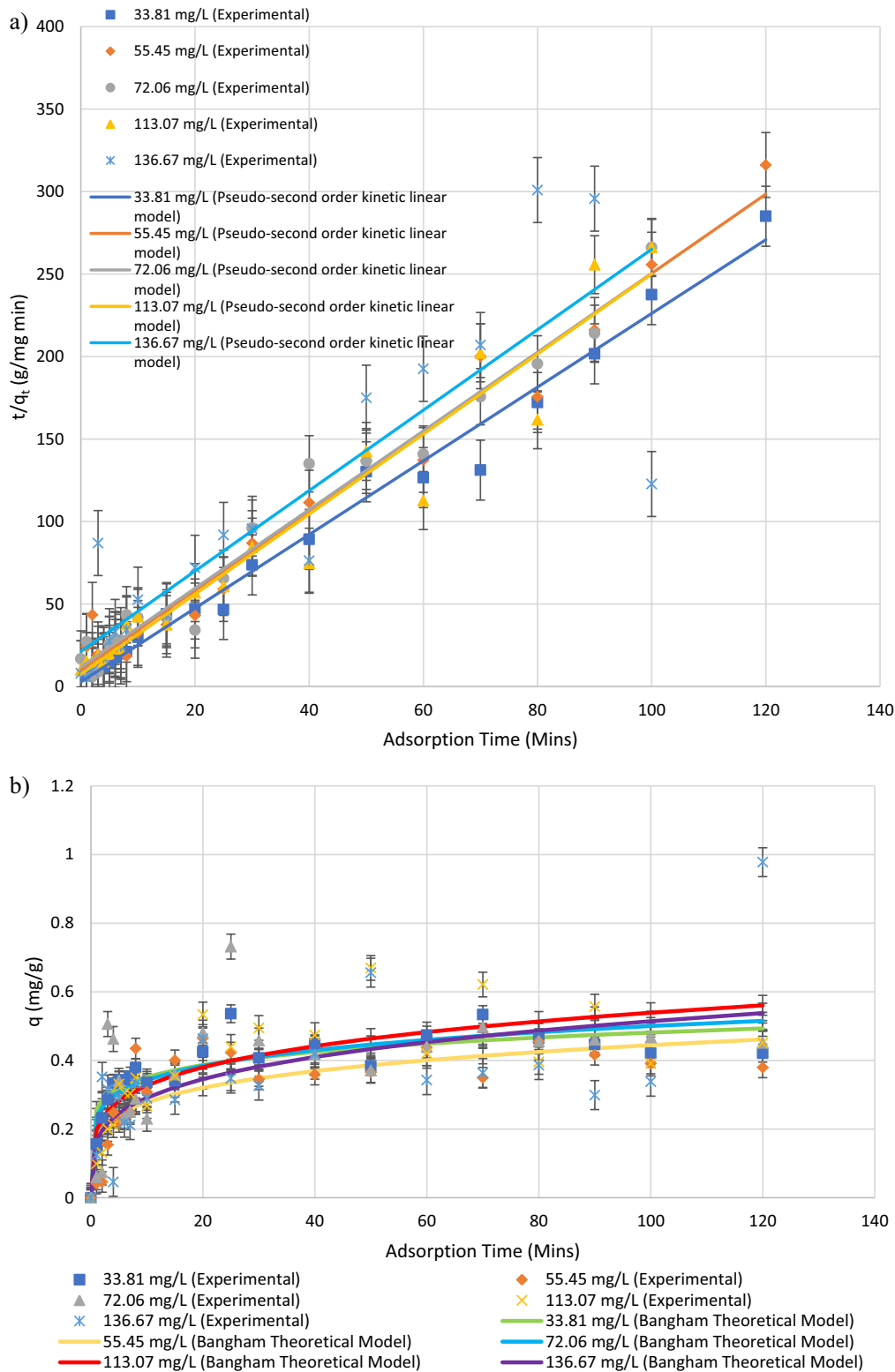


**Fig. 3 a** The linearised form of the pseudo-second-order kinetic model for Reactive Black 5 dye adsorption onto GIC adsorbent. The orange and blue lines represent linear regression analysis; **b** Bangham's kinetic model by non-linear regression method represents the slow rate-limiting step of surface diffusion and intraparticle diffusion of RB5 dye onto GIC adsorbent; **c** The pseudo-first-order

kinetic model by non-linear regression analysis for Reactive Black 5 dye adsorption onto the GIC adsorbent; **d** The pseudo-second-order kinetic model by non-linear regression analysis for Reactive Black 5 dye adsorption onto the GIC adsorbent; **e** The Elovich kinetic model for Reactive Black 5 dye adsorption onto GIC adsorbent; **f** The three-stage kinetic model for RB5 dye adsorption onto GIC adsorbent

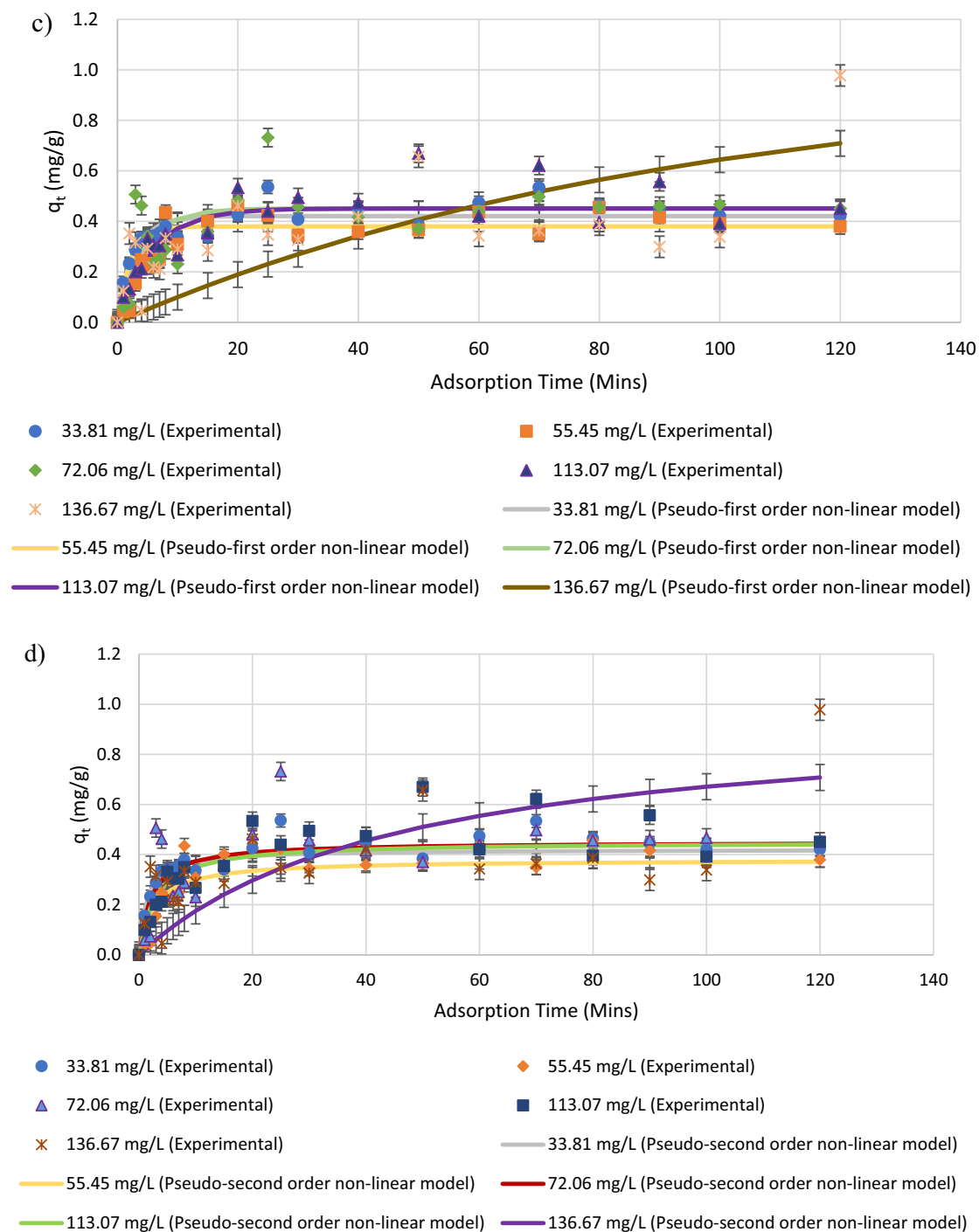


Fig. 3 (continued)

In a kinetic batch system, the adsorbate in the aqueous phase binds to the active sites on the adsorbent surface in a finite system, resulting in the decline of the aqueous phase concentration. In the first two stages of adsorption, the instantaneous adsorption in the first stage involves instantaneous adsorption followed by slow rate-limiting adsorption in the remaining stage as it moves towards the equilibrium

point. The rate-limiting adsorption, which involves the entire mass transfers of adsorbate in the aqueous phase, moves towards the solid phase of the adsorbent through surface diffusion until it fills the active sites of the adsorbent with adsorbate, thereby reaching adsorption equilibrium. The second stage of the adsorption process primarily accounts for time-dependent adsorption, followed by the third stage,

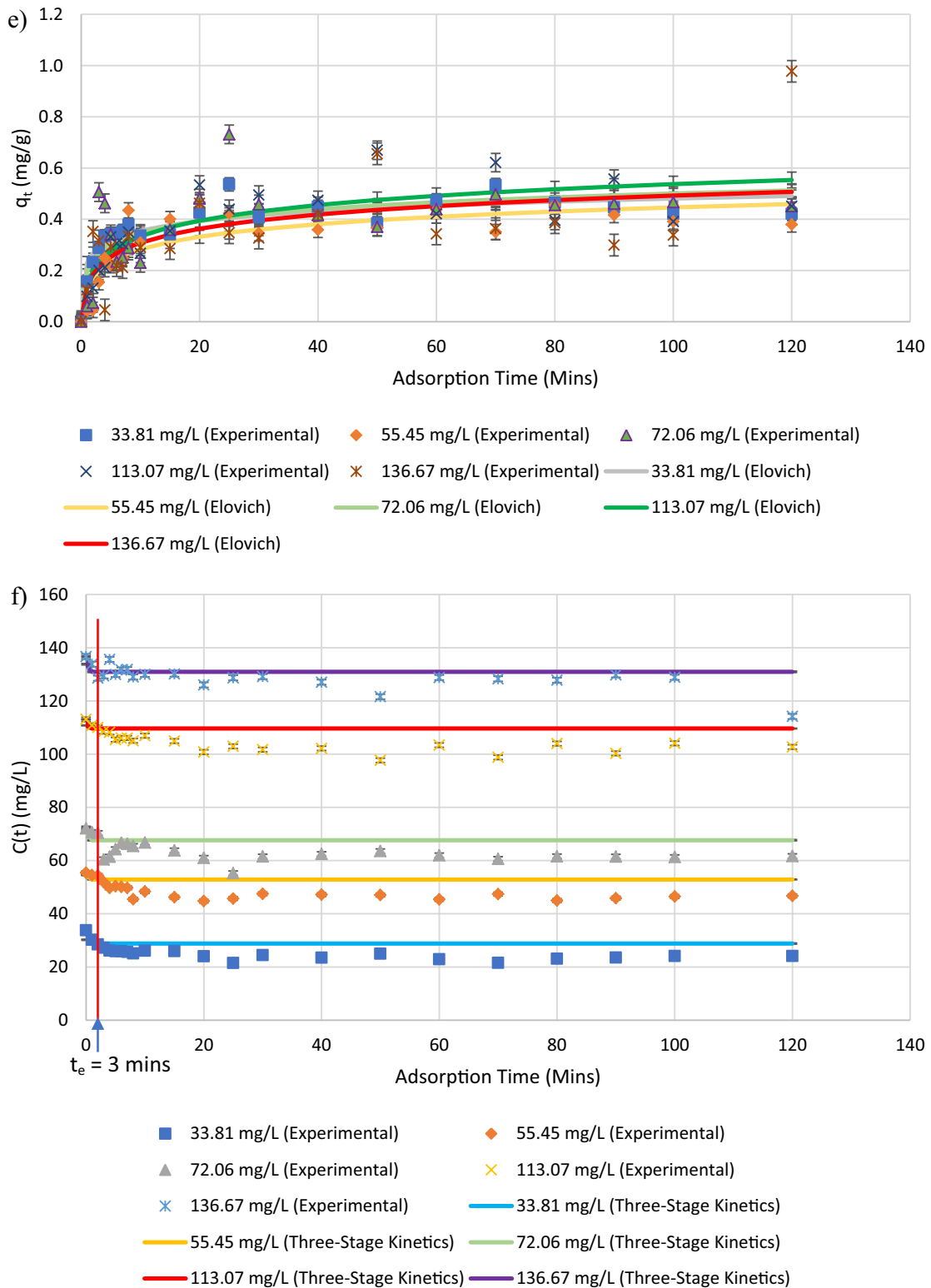


Fig. 3 (continued)

where the aqueous phase concentration remains constant throughout batch adsorption. Furthermore, it can be deduced that the existence of instantaneous adsorption ( $\xi_1$ ) implies

that some portion of the Reactive Black 5 adsorbate was adsorbed onto the external site of the GIC adsorbent within a transient period of time. The higher the initial adsorbate



concentration, especially when the initial dye concentration increased from 33.81 to 136.67 mg/L, resulted in a lower  $\xi_1$  value for both two and three-stage kinetic models. The lower  $\xi_1$  values compared to  $\xi_2$  values, as the initial adsorbate concentration increased, indicated higher intraparticle diffusion. The continuous decrease of the aqueous phase of adsorbate concentration within 2–3 min indicated that the surface diffusion was still ongoing due to the availability of surface area or active sites on the particle size of GIC adsorbent. Due to the continuous decrease in the aqueous phase of adsorbent concentration, the final stage of kinetics had not reached the equilibrium point. Nonetheless, all three stages of kinetic models fitted well with the experimental data, with slight differences between the  $\alpha$  and  $\xi_1$  values for initial adsorbate concentrations ranging between 33.81 and 72.06 mg/L of RB5 dye. Moreover, the higher the initial adsorbate concentration, the more pronounced the three stages, with an especially more distinctive appearance of the second stage due to higher  $q_2(\infty)$  value. This result demonstrated that different adsorption stages largely depend on the initial adsorbate concentration and the adsorbent's physicochemical properties or surface characteristics. The instantaneous adsorption ( $\xi_1$ ) of GIC adsorbent decreased from 0.1064 to 0.0209 as the initial adsorbate concentration increased from 33.81 to 136.67 mg/L. As the initial adsorbate concentration increased, the fast decline in instantaneous adsorption became more pronounced. A high concentration gradient between the bulk liquid solution and the external site of the adsorbent would result in greater surface diffusivity. As the initial adsorbate concentration increased, high competition between adsorbate molecules reduced the number of active sites available for adsorption, resulting in a decrease in  $\beta$  values and, consequently, a reduction in adsorption rate followed by reduced  $\alpha$  values. As the initial adsorbate concentration increased, the instantaneous adsorption portion of the parameter,  $\xi_1$  value decreased while the two-stage parameter,  $\xi_2$  value increased, leading to a longer equilibrium time. Conversely, the higher  $\xi_1$  value, the lower the second-stage adsorption, which may result in a relatively long reaction time until the active sites are filled. However, integrating the third stage model improved the system's flexibility with greater  $\beta$  yields, resulting in a relatively short duration of the second stage. On the other hand, the three-stage kinetic model improved the flexibility of second-stage adsorption by increasing the  $\beta$  yields, thereby compensating the instantaneous portion of  $\xi_1$  and shortening the equilibrium time for the complete reaction. However, a higher  $\beta$  value, especially at initial adsorbate concentration ranging between 33.81 and 136.67 mg/L, indicated limited aqueous mass transfer due to relatively high aqueous phase concentration. For a system with high initial adsorbate concentration and small particle sizes, the three-stage model is more suitable for determining the correct  $\alpha$

value. The instantaneous portion,  $\xi_1$ , increased significantly for both high and low initial adsorbate concentrations, possibly due to particle attrition. The increase in the instantaneous portion,  $\xi_1$ , resulted in a smaller  $\xi_2$  value, which indicated that a higher instantaneous portion inadvertently reduced the second-stage reaction duration. Moreover, the increase in the instantaneous portion,  $\xi_1$ , strongly indicated RB5 adsorbed onto GIC. On the other hand, using a high mechanical stirring rate, significantly greater than 700 rpm, can result in particle attrition, leading to small particle sizes. Small particles have a high surface area, resulting in high instantaneous adsorption. The continuous adsorption–desorption cycles can affect the  $\beta$  value. In contrast, changes in  $\gamma$  values indicated prolonging or shortening reaction times, especially for the third stage. The balance between  $\alpha$  and  $\beta$  values can be discerned through the presumption that the system may experience mass losses from the solution due to the mineralisation process.

Furthermore, the Elovich equation was initially used to examine the adsorption processes and is suitable for systems involving heterogeneous adsorbing surfaces (Wu et al. 2009). The characteristic curve of the Elovich equation resembles those of Lagergren's first-order equation and intraparticle diffusion model (Wu et al. 2009). The data obtained from Table 2 shows that Elovich kinetic model is the best fit for the experimental data. Moreover, Elovich kinetic model is the most appropriate model to describe the adsorption kinetics of RB5 with  $R^2$  values greater than 0.9999. In addition, Fig. 3e shows the rapid rising to instant approaching equilibrium of the low-lying characteristic curve, which indicates rapid adsorption kinetics. The increasing surface diffusion flux driven by a large concentration gradient between solid–liquid interphase facilitated the rapid diffusion of RB5 adsorbate onto the surface of GIC, resulting in fast-approaching equilibrium. In addition, Fig. 4 shows the point of zero charge,  $\text{pH}_{\text{pzc}}$  relative to solution pH on the ionisation of GIC adsorbent.

## Adsorption isotherms

Various isotherm models concerning Fig. 5 are stipulated in this subsection. The Langmuir adsorption isotherm assumes that a homogenous monolayer exists on the surface of the adsorbent, with no interaction between the adsorbed molecules and its neighbouring adsorption sites (Elemile et al. 2022). Moreover, Langmuir adsorption isotherm was initially developed to describe gas–solid interphase adsorption on both carbon and graphite-based adsorbent. This isotherm model is usually based on two common assumptions: 1) the forces of interaction between adsorbed molecules are negligible, and once an adsorbate occupies an active site on the surface of the adsorbent, no further sorption takes place. In addition, Langmuir isotherm refers to homogenous

**Table 2** Summary of linear and non-linear kinetic parameters for adsorption of RB5 dye onto GIC adsorbent

Adsorption Kinetics parameters for Reactive Black 5 dye onto GIC adsorbent by using the pseudo-first-order non-linear equations

$C_0$ (mg/L)	$q_{e,exp}$ (mg/g)	$k_1$ (min <sup>-1</sup> )	$q_{e,cal}$ (mg/g)	$R^2$
33.81	0.4210	0.8014	0.4210	0.9984
55.45	0.3796	1.1009	0.3796	0.9899
72.06	0.4509	0.5417	0.4509	1.0000
113.07	0.4509	0.4012	0.4509	0.9968
136.67	0.9777	0.0248	0.7089	0.9925
Pseudo-first-order equation	Non-Linear Form		Plot	
	$A = e^{\left(\frac{k_1 t}{2.303}\right)} q_e = \frac{-q_t A}{(1-A)}$		$q_t$ versus $t$	

Adsorption kinetics parameters for Reactive Black 5 dye onto GIC adsorbent using the pseudo-second-order linear equations

$C_0$ (mg/L)	$q_{e,exp}$ (mg/g)	$k_2$ (g/mg min)	$q_{e,cal}$ (mg/g)	$R^2$
33.81	0.4210	2.0166	0.2712	0.9869
55.45	0.3796	0.6807	0.2521	0.9781
72.06	0.4509	0.4158	0.2532	0.9754
113.07	0.4509	0.6631	0.2488	0.9500
136.67	0.9777	0.0493	0.2476	0.7603
Pseudo-second-order equations	Linear Form		Plot	
	$\frac{t}{q_t} = \frac{1}{k_2 q_e^2} + \frac{1}{q_e} t$		$\frac{t}{q_t}$ versus $t$	

Bangham kinetic parameters by non-linear regression method for Reactive Black 5 dye adsorption onto GIC adsorbent

$C_0$ (mg/L)	$q_{e,exp}$ (mg/g)	$k$ (min <sup>-1</sup> )	$\theta$	$q_{e, cal}$ (mg/g)	$R^2$
33.81	0.4210	0.2574	0.1358	0.4932	0.9999
55.45	0.3796	0.1744	0.2032	0.4615	0.9710
72.06	0.4509	0.2352	0.1638	0.5154	0.9999
113.07	0.4509	0.1987	0.2167	0.5607	0.9999
136.67	0.9777	0.1651	0.2467	0.5379	0.9999
Bangham Equation	Non-Linear Form			Plot	
	$q = kt^\theta$			$\log_e(Q)$ versus $\log_e(t)$	

Adsorption kinetics parameters for Reactive Black 5 dye onto GIC adsorbent by using the pseudo-second-order non-linear equations

$C_0$ (mg/L)	$q_{e,exp}$ (mg/g)	$k_2$ (min <sup>-1</sup> )	$q_{e,cal}$ (mg/g)	$R^2$
33.81	0.4210	1.8148	0.4164	0.9945
55.45	0.3796	0.9969	0.3714	0.9968
72.06	0.4509	1.0761	0.4433	0.9996
113.07	0.4509	0.7819	0.4405	0.9873
136.67	0.9777	0.0224	0.7079	0.9957
Pseudo-second-order equation	Non-Linear		Plot	
	$q_t = \frac{q_e^2 k_2 t}{1 + q_e k_2 t}$		$q_t$ versus $t$	

Kinetics parameters for adsorption of Reactive Black 5 dye on GIC by using the Three-stage kinetic model

$C_0$ (mg/L)	$q_1$ (t) (mg/g)	$q_2$ (t) (mg/g)	$\alpha$	$\beta$	$\gamma$	$\xi_1$	$\xi_2$	$R^2$
33.81	0.1564	0.4210	0.1711	0.1461	3.4830	0.1064	0.2864	0.9550
55.45	0.0414	0.3796	0.2254	0.1839	7.4240	0.0172	0.1574	0.9547
72.06	0.0598	0.4509	0.4132	0.2924	9.2199	0.0191	0.1439	0.9547
113.07	0.0989	0.4509	0.1266	0.1124	11.9101	0.0201	0.0917	0.9546
136.67	0.1242	0.9777	0.1457	0.1272	6.6720	0.0209	0.1645	0.9546

**Table 2** (continued)

Kinetics parameters for adsorption of Reactive Black 5 dye on GIC by using the Three-stage kinetic model										
$C_0$ (mg/L)	$q_1$ (t) (mg/g)	$q_2$ (t) (mg/g)	$\alpha$	$\beta$	$\gamma$	$\xi_1$	$\xi_2$	$R^2$		
Three-Stage Kinetic Equation		$q_1(t) \equiv q_1(0) \equiv q_1(\infty) \frac{\partial C}{\partial t} = -\alpha C \left[ 1 - \frac{q_2(t)}{q_2(\infty)} \right]$ $q(t) = q_1(t) + q_2(t)$ $\frac{\partial C}{\partial t} = -\alpha C \left[ 1 - \frac{q_2(t)}{\beta q_2(\infty)} \right] VC(t) + M [q_1 + q_2] = VC_0$ $\frac{C(t)}{C_0} = \frac{(1-\xi_1)(1-\xi_1-\beta\xi_2)}{(1-\xi_1-\beta\xi_2 \exp[-\gamma t])}$ $\xi_1 = \frac{Mq_1(\infty)}{VC_0}$ $\xi_2 = \frac{Mq_2(\infty)}{VC_0}$ $\gamma = \frac{(1-\xi_1-\beta\xi_2)\alpha}{\beta\xi_2}$				Plot	$C(t)$ versust			
Elovich kinetic parameters for adsorption of Reactive Black 5 dye onto GIC adsorbent										
$C_0$ (mg/L)	$q_{e,exp}$ (mg/g)	$\alpha$	$\beta$	$q_{e,cal}$ (mg/g)	$R^2$					
33.81	0.4210	3.6758	18.3320	0.4908	0.9999					
55.45	0.3796	0.3652	13.9796	0.4592	0.9999					
72.06	0.4509	1.2161	15.0065	0.5126	0.9999					
113.07	0.4509	0.3677	11.2163	0.5533	0.9999					
136.67	0.9777	0.35422	12.3529	0.5072	0.9999					
Elovich Kinetic Equation		$q_t = \frac{1}{\beta} \ln(\alpha\beta t + 1)$				Plot		$q_t$ versus $t$		

adsorption with a second assumption that there is no transmigration of the adsorbate molecules in the plane perpendicular to the surface of the adsorbent (Shahbeig et al. 2013). This isotherm model has the following hypotheses (Shahbeig et al. 2013):

- (1) The monolayer adsorption is approximately one molecule in thickness.
- (2) Adsorption usually takes at specific homogenous active sites within the surface of the adsorbent.
- (3) Once an adsorbate occupies an active site, no further sorption takes place at that particular site.
- (4) The free energy at the adsorption site is relatively constant and independent of the degree of adsorbate occupation on the active site of the adsorbent.

- (5) The strength of attractive intermolecular forces depends on the distance between the adsorbate molecule and the active site of the adsorbent, indicating that the further away the adsorbate is from the adsorbent surface, the lower the attraction.
- (6) The physicochemical structure of the adsorbent is considered to be homogeneous.

However, the Langmuir isotherm model's main limitation is its validity in low-pressure constraints. Another drawback of Langmuir isotherm is that it assumes uniform monolayer adsorption of adsorbate or solute at a specific homogenous active site. In reality, this rarely occurs in the presence of high adsorbate concentration, which results in rapid saturation of active sites caused by competition adsorption phenomena or interaction between adsorbates on different active sites. The ongoing adsorption and desorption processes affect the accuracy of the assumption for a mechanistic model.

Two significant assumptions are related to the derivation of Temkin isotherm (Chu 2021): (1) There is a uniform distribution of heterogeneous binding sites on the solid surface; (2) The binding energy varies linearly over different binding sites. Temkin isotherm is often used to characterise the environmental adsorption of contaminants, but it suffers from dimensional inconsistency (Chu 2021). The dimensionally inconsistent formulation, as shown in Table 3, may affect the accuracy of the representation of fitted theoretical data against the experimental data. Two undesirable features relate to the fitted curve: (1) any initial dye concentration beyond 100 mg/L does not accurately predict the saturation

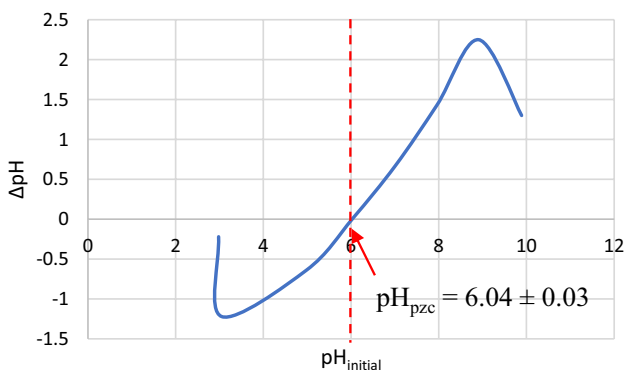


**Fig. 4** Point of zero charge of GIC particle electrode

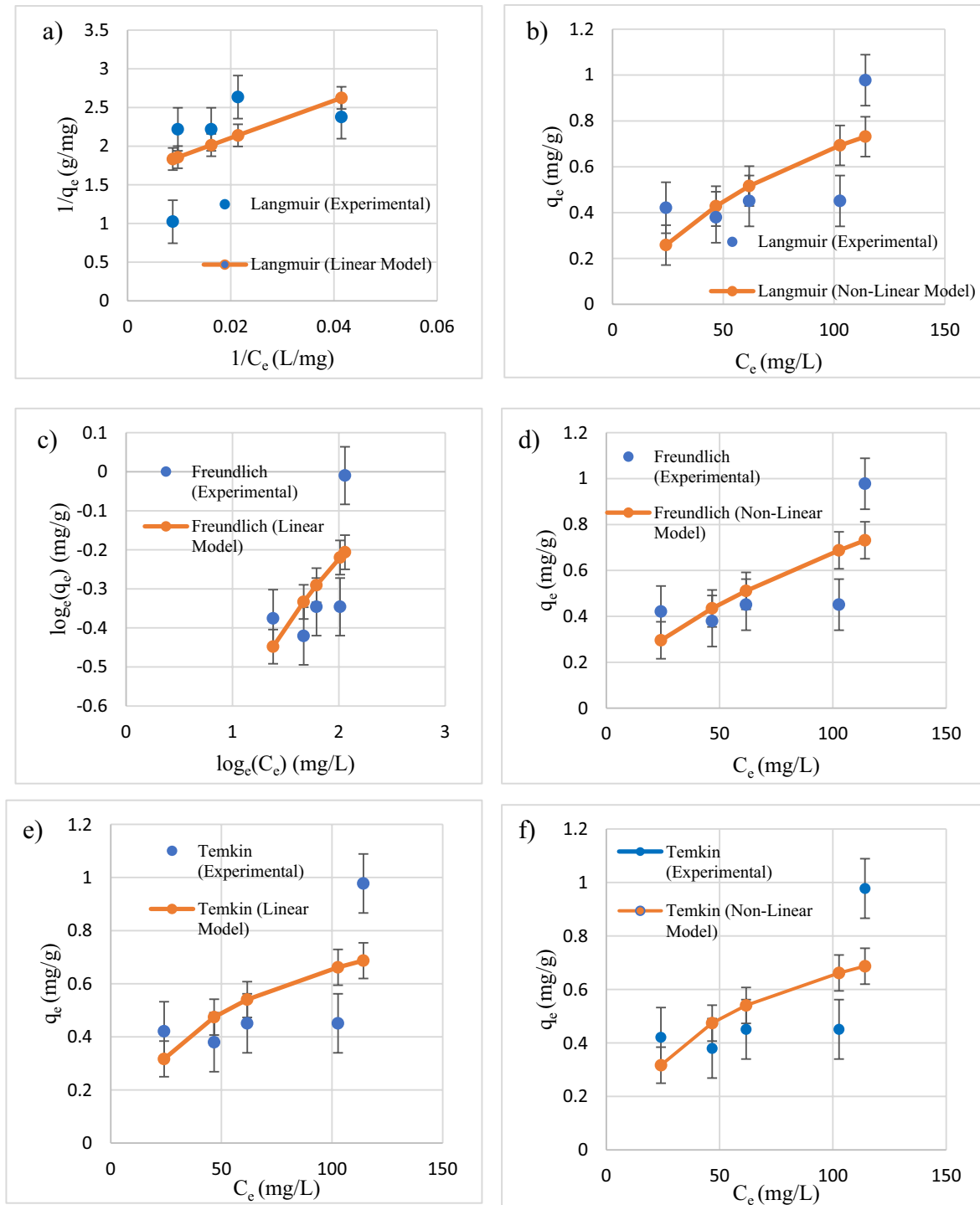


**Fig. 5** **a** Langmuir adsorption isotherm for RB5 onto GIC adsorbent by linear regression method; **b** Langmuir adsorption isotherm for RB5 onto GIC adsorbent by non-linear regression method; **c** Freundlich adsorption isotherm for RB5 onto GIC adsorbent by linear regression method; **d** Freundlich adsorption isotherm for RB5 onto GIC adsorbent by non-linear regression method; **e** Temkin adsorption isotherm for RB5 onto GIC adsorbent by linear regression method;

**f** Temkin adsorption isotherm for RB5 onto GIC adsorbent by non-linear regression method; **g** SIPS adsorption isotherm for RB5 onto GIC adsorbent by linear regression method; **h** SIPS adsorption isotherm for RB5 onto GIC adsorbent by non-linear regression method; **i** Redlich–Peterson isotherm modelling by linear regression method; **j** Redlich–Peterson adsorption isotherm for RB5 onto GIC adsorbent by non-linear regression method



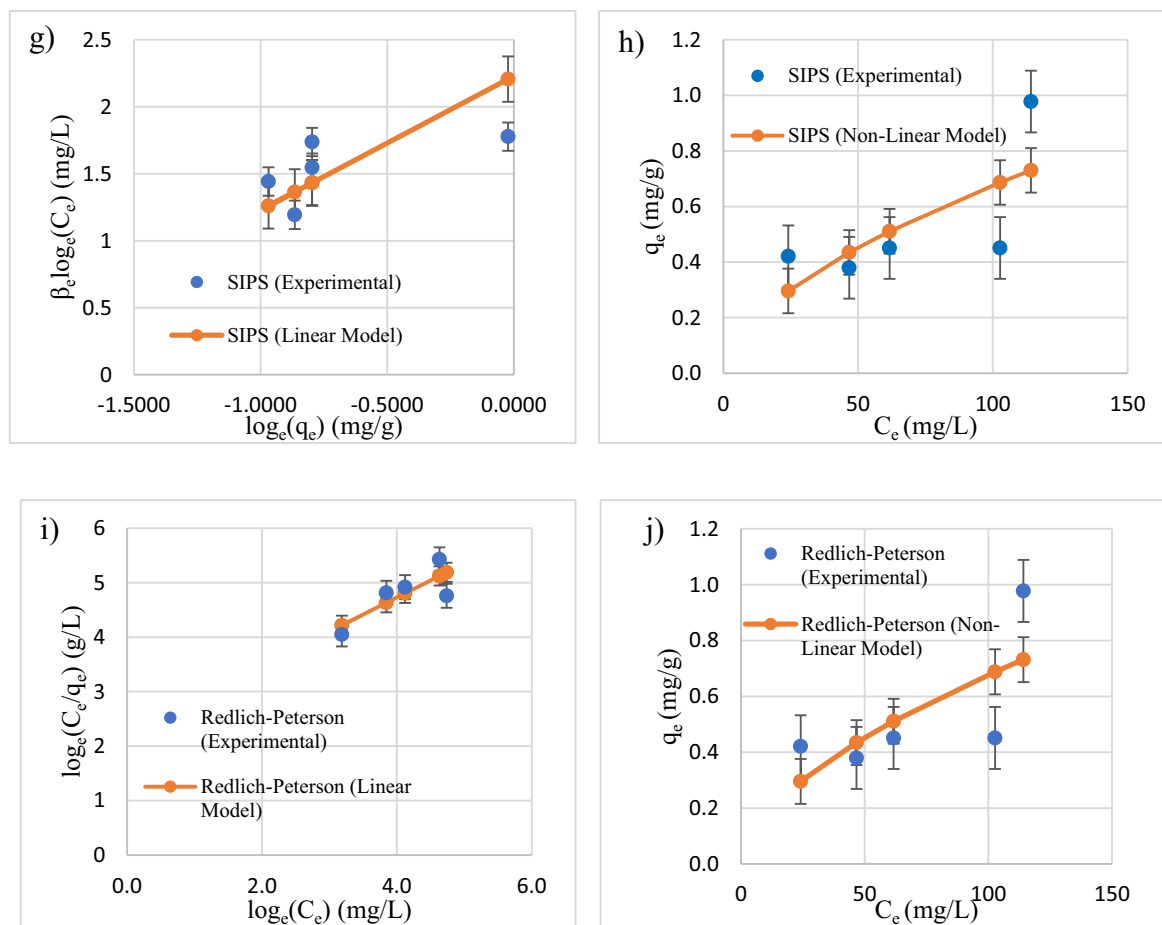


Fig. 5 (continued)

limit, especially at high concentrations, resulting in more significant disparities between theoretical and experimental data; (2) The second undesirable feature is present in both low and high regions. This indicates that the experimental values are less than the accepted values, giving the average relative errors negative values. Nonetheless, the inherent deficiencies in Temkin formulation do not entirely restrict its ability to correlate the equilibrium data to a significant degree of precision. In other words, the fitting of the Temkin equation to an equilibrium data and experimental profile is still within a validity range despite some minor deviations at both high and low concentrations. Some minor deviations could be attributed to the ongoing desorption process within the adsorption system.

Furthermore, SIPS isotherm combines Langmuir and Freundlich models and is appropriate for characterising heterogeneous adsorption systems at various pressures and temperatures (Tzabar and ter Brake 2016). The SIPS model has been found to fit liquid adsorption data remarkably well,

especially for liquid–solid adsorption systems. Although the results showed that the adsorption systems are suitable for RB5 contaminant, the apparent SIPS formulation may conceal problematic application issues. The application issues are expounded as follows (de Vargas Brião et al. 2023): (1) the dubious practice of using linear versions of the SIPS equation to fit the experimental profile; (2) the inherent mismatches between the SIPS and Langmuir–Freundlich equations; and (3) the trivial practice of correlating the SIPS equation to experimental data. To overcome the inherent deficiencies, SIPS combined the characteristics of the Freundlich model to assume that the amount of adsorbate increases indefinitely with pressure, resulting in a distribution function correlated with an increase in the infinite number of active sites available for adsorption.

On the other hand, SIPS derived another distribution function to predict a finite number of active sites available on the adsorbent surface. To make this derivation method workable, SIPS incorporated exponent  $n$ , ranging between 0

**Table 3** Summary of linear and non-linear parameters for isotherm models for the adsorption of RB5 dye onto GIC adsorbent

Linear and non-linear parameters of isothermal models for the sorption of Reactive Black 5 (RB5) dye onto GIC adsorbent				
Two-parameter isotherms				
Isotherm models	Linear method		Non-linear method	
Langmuir	$q_m$ (mg/g)	0.6166	$q_m$ (mg/g)	1.4369
	B	0.0671	b	0.0091
	$R^2$	1.0000	$R^2$	0.9992
	$\frac{1}{q_e} = \left(\frac{1}{bq_m}\right)\frac{1}{C_e} + \frac{1}{q_m}$		$q_e = \frac{bK_L C_e}{1+bC_e}$	
Freundlich	$K_F$ (L/mg)	0.2263	$K_F$ (L/mg)	0.0464
	n	0.7133	n	1.7179
	$R^2$	1.0000	$R^2$	0.9999
	$\log_e(q_e) = \log_e(K_F) + \frac{1}{n} \log_e(C_e)$		$q_e = K_F C_e^{\frac{1}{n}}$	
Temkin	A	0.1568	A	0.1568
	B	0.2381	B	0.2381
	$R^2$	1.0000	$R^2$	1.0000
	$q_e = \frac{RT}{b} \log_e(A) + \frac{RT}{b} \log_e(C_e)$		$q_e = B \log_e(AC_e)$	
	$\beta = \frac{RT}{b}$		$\beta = \frac{RT}{B}$	
Three-parameter isotherms				
Isotherm models	Linear method		Non-linear method	
SIPS	$q_m$	0.0176	$q_m$	84.9456
	$K_s$ (L/g)	0.0019	$K_s$ (L/g)	$2.5727 \times 10^{-6}$
	n	0.3751	n	0.5840
	$R^2$	1.0000	$R^2$	0.9999
	$\beta_s \log_e(C_e) = -\log_e\left(\frac{K_s}{q_e}\right) + \log_e(\alpha_s)$		$q_e = q_m \left( \frac{K_s C_e}{1 + K_s C_e} \right)^n$	
Redlich–Peterson	A	0.1076	A	5.2680
	$\beta$ (L/mg)	0.6249	B (L/mg)	113.5293
	$R^2$	0.9999	$\beta$	0.4176
		$\log_e\left(\frac{C_e}{q_e}\right) = \beta \log_e(C_e) - \log_e(A)$		$R^2$
			$q_e = \frac{AC_e}{1+BC_e^\beta}$	

and 1, to make the adsorption systems more manageable at an extensive range of pressures. Since Freundlich isotherm only approximates the adsorption behaviour of the system, the value of  $1/n$  can only range between 0 and 1; therefore, the equation only accounts for a limited range of pressure. Given the status of adsorption systems, the Langmuir–Freundlich equation is interconvertible with the SIPS formulation (de Vargas Brião et al. 2023). No meaningful insights can be gained by fitting the Langmuir–Freundlich and SIPS equations separately to similar experimental data sets and comparing their degrees of precision. Hence, the SIPS equation may lack mechanistic relevance.

More interestingly, a three-parameter Redlich–Peterson isotherm equation is introduced to amend the inaccuracies and inherent deficiencies of two-parameter Langmuir

and Freundlich isotherm equations. The Redlich–Peterson isotherm equation is more accurate than Langmuir and Freundlich equations in describing the adsorption systems using GIC adsorbent, which is consistent with Wu et al. (2010). Unlike Langmuir and Freundlich isotherms, the Redlich–Peterson isotherm equation incorporates additional parameters such as A, B and  $\beta$  to increase the accuracy and precision of curve fitting between analytical and experimental data. Moreover, the Redlich–Peterson isotherm balances the Langmuir and Freundlich systems and incorporates the benefits of both models rather than conflicts between the two systems. In addition, the degree of curve fitting for linearity and non-linearity of isotherm equations depends on the types of experimental adsorption systems. Occasionally, a linearised form of an isotherm

equation may yield a better fit for experimental data than a non-linearised form of equation, depending on the type of adsorption system.

According to Table 3, the sum of the squares error (ERRSQ/SSE) values for Redlich–Peterson and SIPS isotherms were the lowest compared to other values of isotherm models, resulting in a better fit between theoretical and experimental data. Although ERRSQ/SSE is the most widely reported error function in isotherm modelling, the major disadvantage is its poor error prediction at high-pressure conditions, which may reflect the true nature of adsorption complexity (Serafin and Dziejarski 2023). The hybrid fractional error function (HYBRID) was initially developed to improve the curve fitting of the sum of squares error (ERRSQ/SSE) to account for low relative pressure condition by dividing it by the measured experimental values at equilibrium condition (Serafin and Dziejarski 2023). The hybrid fractional error function (HYBRID) was selected as the optimal error function to ascertain and analyse the isotherm models to characterise the finest fit between theoretical and experimental data. In addition, the sum of absolute errors (SAE) is a similar error function to ERRSQ/SSE, confirming that non-linear, three-parameter Redlich–Peterson and SIPS isotherm models provided the finest fit between theoretical and experimental data. In Table 3, it was observed that the hybrid fractional error function for Redlich–Peterson and SIPS isotherms, in conjunction with the chi-square test ( $\chi^2$ ), yielded the overall best-fitting performance compared to other isotherm models. It can be deduced that HYBRID and  $\chi^2$  error function analyses are significant tools in evaluating the isotherm modelling because they are statistically robust and well-established measurement tools for accurate curve-fitting models. The benefits of having both HYBRID and  $\chi^2$  error function analyses are due to balances between the influence of both large and small error values in HYBRID measurement, whereas comparative evaluation of model deviation between predicted and experimental values by taking into account the uncertainty in experimental modelling in  $\chi^2$  error function analysis. Based on this reasoning, HYBRID and  $\chi^2$  error functions provided the best principal method for determining and analysing the accuracy and precision of isotherm models to yield the finest curve fitting between theoretical and experimental data. Among other error functions, Marquardt's percent standard deviation (MPSD) measures the geometric mean of the error distribution modified in accordance with the degrees of freedom in the isotherm models (Serafin and Dziejarski 2023). On the other hand, Marquardt created the average relative error (ARE) to minimise the fractional error in statistical distribution over a range of relative pressure conditions (Serafin and Dziejarski 2023). The chi-square values of Redlich–Peterson and SIPS were approximately 0.9925 compared to chi-square values of 0.2769 and 0.1472 for Langmuir and Freundlich isotherm models, respectively. Hence, the

larger the chi-square values, the greater the probability that the isotherm models were statistically significant, indicating that Redlich–Peterson and SIPS isotherm models were a better fit for the experimental data compared to Langmuir and Freundlich isotherm models. The coefficient of determination was calculated using Excel Solver Add-In (2022). In terms of mechanistic phenomena, the predicted amount of adsorbed adsorbate reached an equilibrium state closely resembling the observed amount of adsorbed adsorbate at the equilibrium state, thereby validating the predictability of isotherm models to describe the experimental data. On the other hand, the G-statistic values for Redlich–Peterson and SIPS isotherm models were 0.4682 and 0.4683, respectively. Hence, it indicated that the deviance for the isotherm models from the experimental data was statistically significant compared to Langmuir and Freundlich isotherm models with G-statistic values of  $-6.5832$  and  $-7.5650$ , respectively. Hence, this indicated that the Redlich–Peterson and SIPS isotherm models had better goodness-of-fit.

In contrast, Langmuir and Freundlich's deviance for the predicted models and experimental data was significantly smaller than expected, indicating that the comparative models were statistically insignificant. Unlike the actual goodness-of-fit test, the G-statistic test does not calculate the probability of obtaining the experimental results from something more extreme. Instead, it utilizes the experimental data to calculate a test statistic to determine how far the experimental data deviates from the theoretical results based on null expectation. To support this mathematical relationship, the chi-square calculation is then used to estimate the probability of obtaining that value of the G-test statistics. This indicated that the G-test statistic is more efficient than the chi-square test in measuring the goodness-of-fit, provided that the values between the experimental and theoretical data must be statistically significant or contingent upon the overall significance of the models (Osorio et al. 2024). In Table 4, MPSD errors for Redlich–Peterson and SIPS isotherms were the lowest compared to other isotherm models, verifying the statistical significance of HYBRID and  $\chi^2$  error function tools, indicating the best curve fitting characteristics of the isotherm models. Hence, the following is the categorisation of error functions based on the findings obtained from the RB5 adsorption system, starting from the left with the error function that provides the best curve fitting between the experimental and theoretical isotherm models:

$$\chi^2 > \text{HYBRID} > \text{ERRSQ/SSQ} > \text{ARE} \\ > \text{EABS} > \text{MPSD} > \sigma > R^2$$

In contrast to two-parameter isotherm models, the three-parameter isotherm models were characterised by relatively low HYBRID and ERRSQ/SSE values. In accordance with HYBRID,  $\chi^2$  and ERRSQ/SSE, the degrees of curve fitting of all isotherm models are ranked in the following order:

**Table 4** Error function analysis for six isotherm equations for comparison between experimental and theoretical data

Error functions	R <sup>2</sup>	Coefficient of non-determination	R <sub>adj</sub> <sup>2</sup>	σ	Standard Error	ERRSQ/SSE	ARE	HYBRID	EABS	MPSD	Chi-square (χ <sup>2</sup> )	G-test
<b>Linear approach</b>												
<b>Two-parameter isotherms</b>												
Langmuir	1.0000	0.0000	1.0000	0.2620	0.2620	0.2620	0.2060	0.2036	7.8964	0.2512	0.2434	0.9839
Freundlich	1.0000	0.0000	1.0000	0.2342	0.2342	0.2342	0.1645	-2.2266	-5.9376	0.1225	0.3353	0.9913
Temkin	1.0000	0.0000	1.0000	0.2286	0.2286	0.1568	-4.6303	-12.3474	0.0000	0.3957	0.9924	0.2514
<b>Three-parameter isotherms</b>												
Redlich–Peterson	0.9999	0.0000	0.9999	0.2275	0.2275	0.1553	-3.3954	-5.6590	0.1169	0.3303	0.9925	0.4683
SIPS	0.9999	0.0000	0.9999	0.2275	0.2275	0.1553	-3.3938	-5.6563	0.1170	0.3303	0.9925	0.4683
<b>Non-linear approach</b>												
<b>Two-parameter isotherms</b>												
Langmuir	0.9992	0.0008	0.9970	0.2255	0.2255	0.1530	-3.4031	-5.6718	0.0535	0.4239	0.9910	0.3792
Freundlich	0.9999	0.0001	0.9995	0.2153	0.2153	0.1390	-5.0728	-8.4546	0.0199	0.3941	0.9940	0.2691
Temkin	1.0000	0.0000	1.0000	0.2286	0.2286	0.1568	-7.4084	-12.3474	0.0000	0.3957	0.9924	0.2514
<b>Three-parameter isotherms</b>												
Redlich–Peterson	0.9999	0.0001	0.9991	0.2637	0.2637	0.1390	-5.0752	-12.6879	0.0196	0.4831	0.9938	0.2686
SIPS	0.9999	0.0001	0.9989	0.2638	0.2638	0.1391	-5.0317	-12.5793	0.0215	0.4818	0.9938	0.2722



Redlich – Peterson > SIPS > Temkin  
> Freundlich > Langmuir

By interpreting the above sequential order, it is evident that Redlich-Peterson and SIPS isotherms are the most appropriate models for verifying research associated with RB5 adsorption systems involving GIC.

### Electrochemical oxidation of reactive black 5

The experimental studies demonstrated that  $12 \text{ mA/cm}^2$  was the minimum current density required to reduce RB5 concentration in water significantly. Both dye and TOC removal percentages increased continuously beyond  $12 \text{ mA/cm}^2$ . This indicated that more intermediate oxidation products were subsequently mineralised into  $\text{CO}_2$  and  $\text{H}_2\text{O}$ . A higher current density of  $45 \text{ mA/cm}^2$  could eventually eliminate residual RB5 in water, resulting in a 93% mineralisation efficiency and 67% TOC removal rate (Fig. 6). In addition, electrolysis can effectively remove RB5 from water by destroying its molecular structure through the cleavage of azo bonds. However, some RB5 molecules may not be wholly mineralised into inert  $\text{CO}_2$  and  $\text{H}_2\text{O}$ . In addition, Fig. 6 represents the effect of current density on the mineralisation and RB5 removal efficiencies. The greater the current density, the greater the removal efficiencies of RB5 and TOC. On the other hand, Fig. 6 shows the effect of current density on the annual electricity cost for TOC, which

varied due to the buildup of side reactions at a current density greater than  $20 \text{ mA/cm}^2$ . The mineralisation of RB5 molecules into  $\text{CO}_2$  at higher current density also contributed to the loss of intermediate transformation species in water, impacting the ionic conductivity of aqueous media. In terms of technoeconomic analysis, the electricity cost per hour of electrolysis using  $34 \text{ mA/cm}^2$  of current density was amounted to 49.59 AUD/kg of RB5 and 334.52 AUD/kg of TOC. Furthermore, Fig. 7 shows the effect of current density on the electrochemical regeneration efficiency of GIC particle electrodes in the presence of RB5-polluted wastewater. High current density led to surface roughening of the GIC, causing changes in the surface physicochemical properties of GIC. Fresh GICs initially have acidic quinone and carboxyl groups on its surface. Upon electrochemical regeneration, these functional groups increase in quantity. A sustained regeneration leads to the formation of basic lactones, which offsets the relative amounts of acidic functional groups. The increase in adsorption can be attributed to strong surface acidic functionalities. Subsequent adsorption and regeneration cycles lead to a greater formation of basic functional groups, which outnumbers the amount of surface acidic functional groups, reducing adsorption (Nkrumah-Amoako et al. 2014). The presence of anions in the solution may increase the electrostatic repulsive forces between GIC and RB5 molecules at the solid–liquid interface, reducing the ability of GIC to adsorb RB5 effectively.

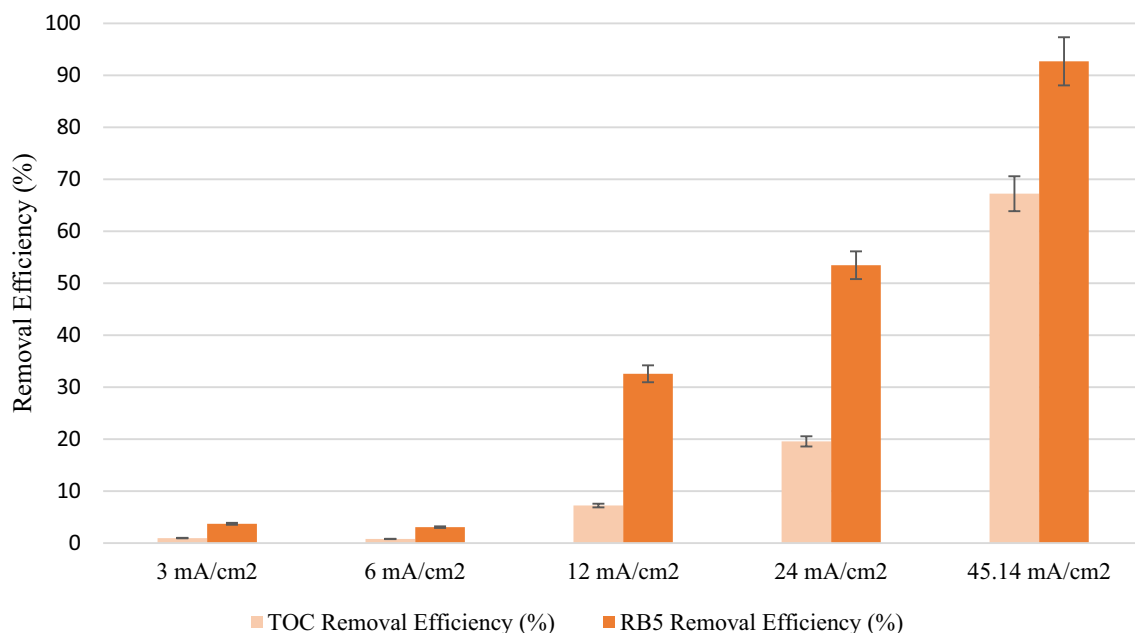


**Fig. 6** Effect of current density on dye and TOC removal efficiencies. Each experiment comprises 20 min of adsorption and 10 min of regeneration at a range of current densities from 3 to  $45.14 \text{ mA/cm}^2$  and 30 V. The error bars represent the coefficient of variation of 2.32%

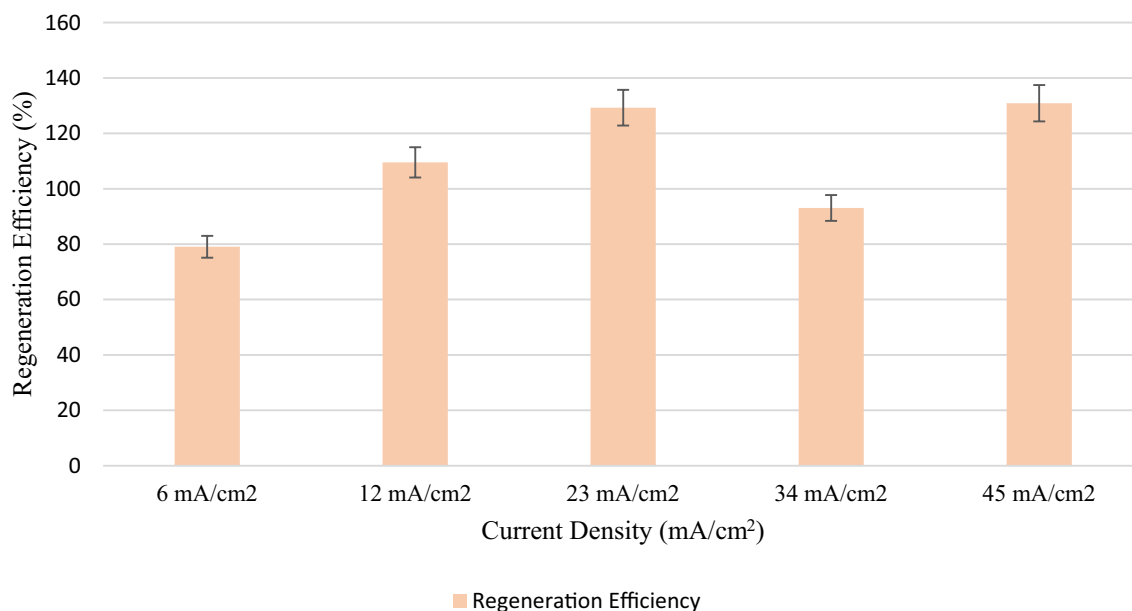


**Fig. 7** Electrochemical regeneration efficiency of GIC particle electrodes in the presence of RB5-polluted wastewater

### Optimisation study using three-dimensional response surface plots

This experimental study investigated the effect of operating parameters such as temperature, pH and salt concentration on the RB5 and TOC removal efficiencies using surface response methodology (Kanneganti et al. 2022) integrated with central composite design (Medeiros et al. 2022). Other constant variables included an initial RB5 concentration of 50 mg/L, an adsorption time of 10 min and an adsorbent dosage of 20 g/L. The batch experimental runs were conducted in accordance with the CCD Design of Experiment to visualize the effects of interactive variables on targeted responses using RSM optimization techniques. A general result demonstrated that when the temperature and pH or salt concentration increased, the RB5 and TOC removal efficiencies also increased as shown in RSM and contour plots of Figs. 8a–j.

The experimental results were evaluated and approximated using the mathematical expressions or functions of various targeted responses, such as dye and TOC removal efficiencies presented in regression equations in coded units:

$$Y_1 = 32.7 - 0.46x_1 - 2.56x_2 - 1.35x_3 - 0.0015x_1x_1 + 0.116x_2x_2 - 0.004x_3x_3 + 0.0493x_1x_2 + 0.0549x_1x_3 - 0.077x_2x_3 \quad (4)$$

$$Y_2 = 12.6 - 0.177x_1 - 1.06x_2 - 0.71x_3 - 0.00064x_1x_1 + 0.0484x_2x_2 - 0.0006x_3x_3 + 0.0181x_1x_2 + 0.0233x_1x_3 - 0.0190x_2x_3 \quad (5)$$

Furthermore, Table 5 shows the ANOVA analysis of RB5 removal efficiency. The F-value of pH variable was 5.60, which was significantly greater than the P-value of 0.039. On the other hand, Table 6 shows the ANOVA analysis for TOC removal efficiency with the F-value of pH variable at 5.90, which was significantly greater than the P-value of 0.036, whereas the F-value of temperature was 0.31 and the P-value was 0.589, indicating that the temperature variable had no significant interactive effect on the overall GIC adsorption efficiency. The following represents the Pareto chart that visualises the interactive effects of various operating variables on the RB5 and TOC removal efficiencies. The Pareto chart in Fig. 9a shows the bars representing one of the independent variables, pH, crosses the reference line with an absolute value of 2.228. This indicates that only pH value produced a statistically significant effect on the dye removal efficiency with less than the  $\alpha$ -value of 0.05. Similarly, the synergistic effect of combined temperature and pH, temperature and salt concentration and pH and salt concentration (AB, AC, BC) etc., did not produce a statistically significant effect on the dye removal efficiency. A similar trend was observed for Fig. 9b, indicating that pH significantly impacted the TOC removal efficiency. Overall results showed that salt concentration had no significant effect on the selectivity reversal of GIC adsorption of RB5 compared to the pH

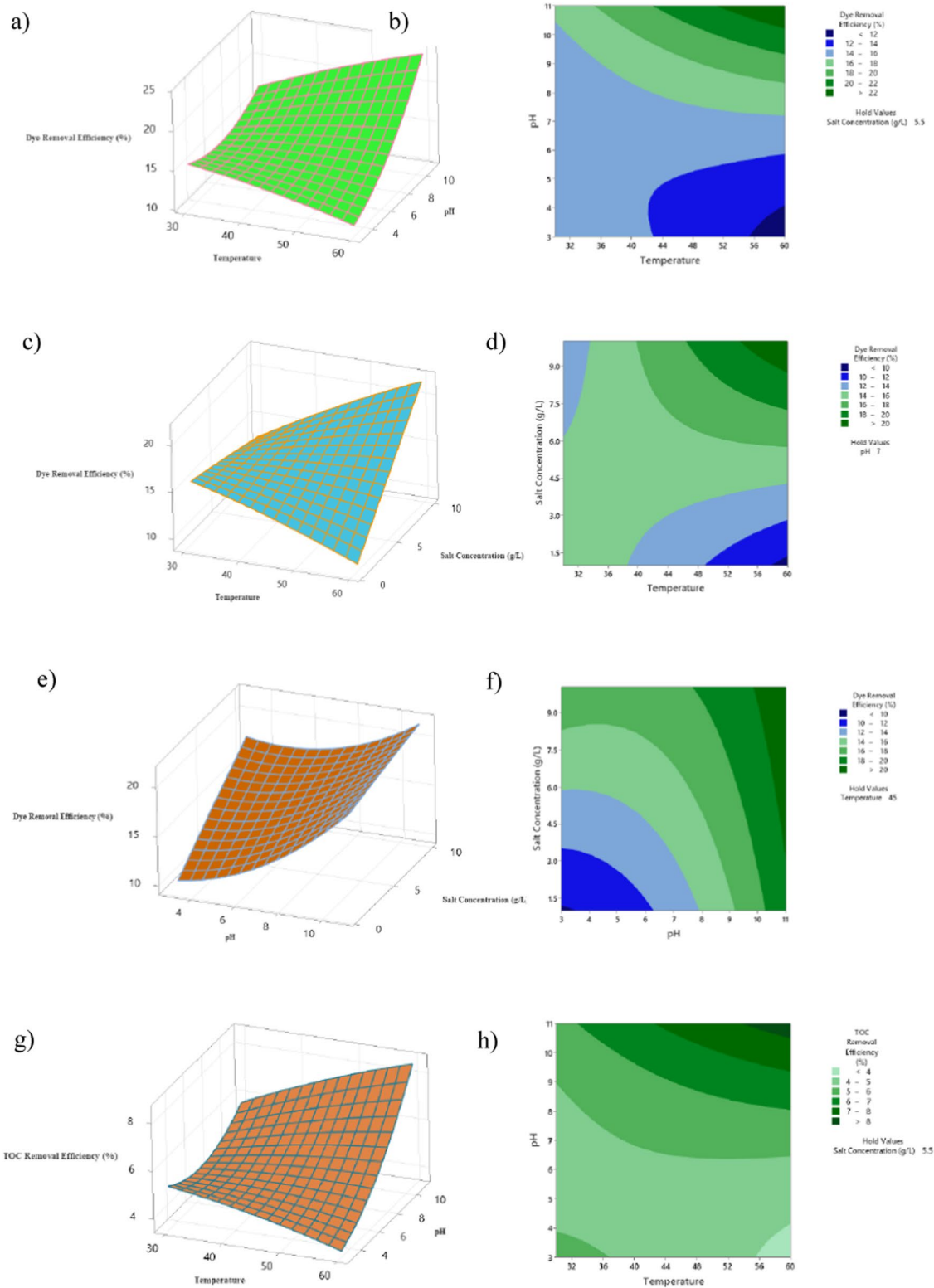


**Fig. 8** 3D RSM optimisation plots of the interaction effects of temperature, pH and salt concentration in a binary mixture with an initial dye concentration, adsorption time and adsorbent dosage of

$C_0=50$  mg/L,  $t=10$  min and adsorbent dosage of 20 g/L, respectively. The actual values of the operating parameters are mean values (coded values 0)

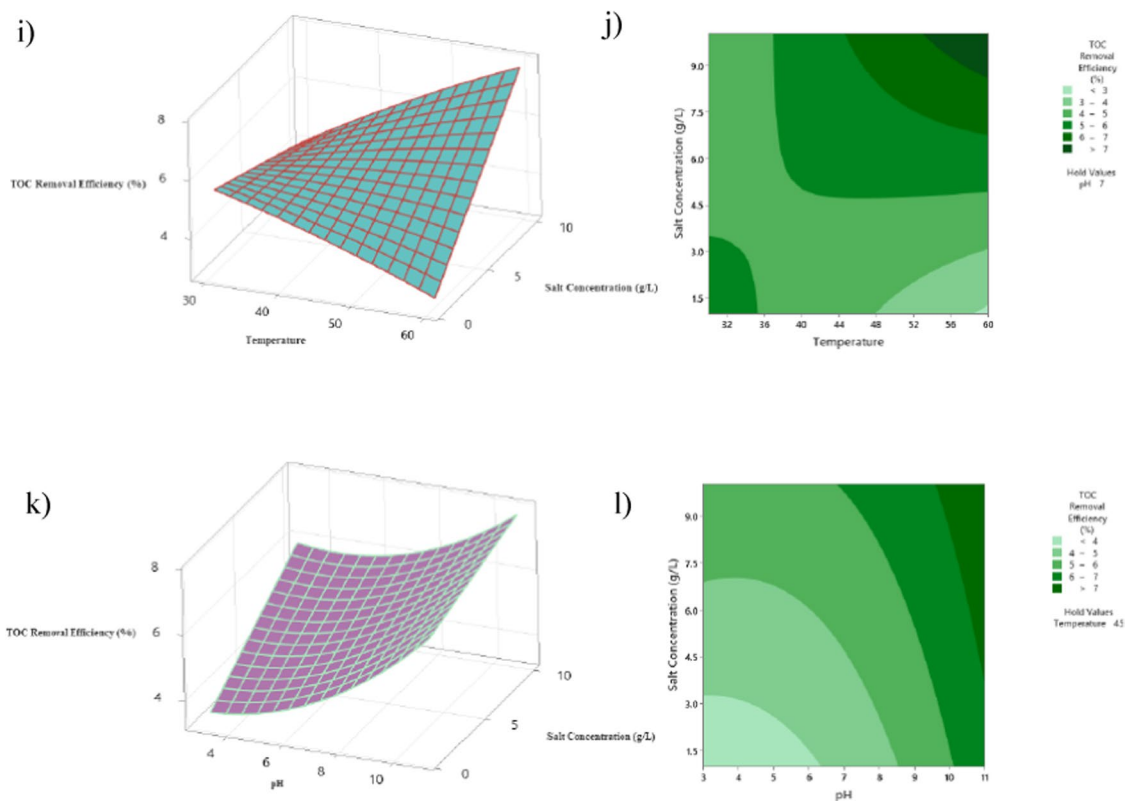


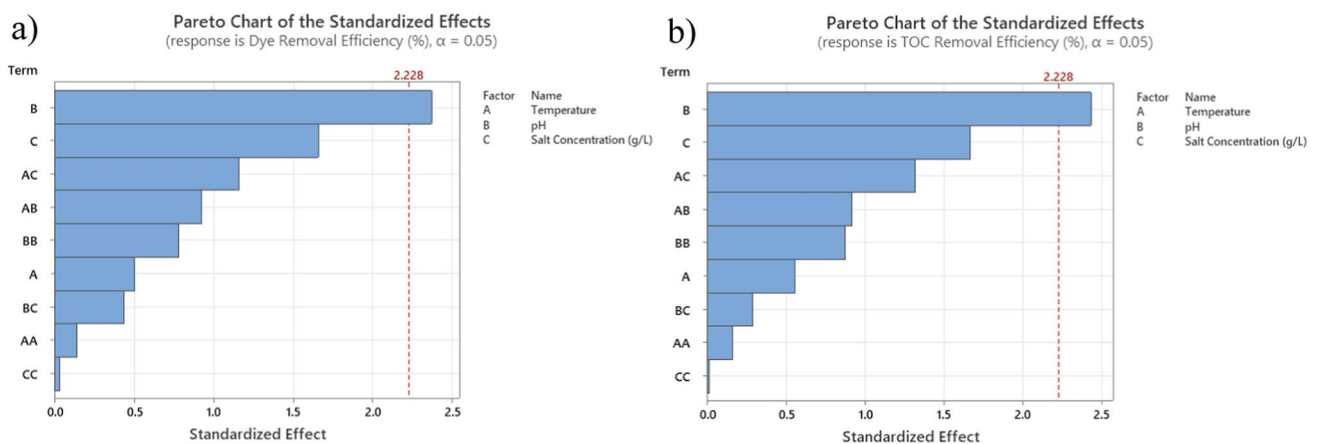
Fig. 8 (continued)

**Table 5** ANOVA analysis of interactive variables on the RB5 removal efficiency

Source	DF	Adj SS	Adj MS	F-Value	P-Value
Model	9	119.095	13.2328	1.30	0.344
Linear	3	87.817	29.2724	2.87	0.090
Temperature	1	2.577	2.5769	0.25	0.626
pH	1	57.194	57.1940	5.60	0.039
Salt Concentration (g/L)	1	28.046	28.0463	2.75	0.128
Square	3	6.818	2.2725	0.22	0.879
Temperature*Temperature	1	0.213	0.2125	0.02	0.888
pH*pH	1	6.227	6.2272	0.61	0.453
Salt Concentration (g/L)*Salt Concentration (g/L)	1	0.010	0.0103	0.00	0.975
2-Way Interaction	3	24.460	8.1534	0.80	0.522
Temperature*pH	1	8.761	8.7614	0.86	0.376
Temperature*Salt Concentration (g/L)	1	13.755	13.7548	1.35	0.273
pH*Salt Concentration (g/L)	1	1.944	1.9440	0.19	0.672
Error	10	102.105	10.2105		
Lack-of-Fit	5	74.423	14.8847	2.69	0.151
Pure Error	5	27.682	5.5364		
Total	19	221.200			

**Table 6** ANOVA analysis for determination of the significance of interactive variables on the TOC removal efficiency

Source	DF	Adj SS	Adj MS	F-value	P-value
Model	9	17.6369	1.95966	1.39	0.308
Linear	3	12.6960	4.23201	3.00	0.082
Temperature	1	0.4407	0.44071	0.31	0.589
pH	1	8.3332	8.33320	5.90	0.036
Salt Concentration (g/L)	1	3.9221	3.92210	2.78	0.127
Square	3	1.1761	0.39205	0.28	0.840
Temperature*Temperature	1	0.0376	0.03764	0.03	0.874
pH*pH	1	1.0783	1.07831	0.76	0.403
Salt Concentration (g/L)*Salt Concentration (g/L)	1	0.0003	0.00026	0.00	0.989
2-Way Interaction	3	3.7648	1.25493	0.89	0.480
Temperature*pH	1	1.1836	1.18359	0.84	0.382
Temperature*Salt Concentration (g/L)	1	2.4637	2.46371	1.74	0.216
pH*Salt Concentration (g/L)	1	0.1175	0.11749	0.08	0.779
Error	10	14.1232	1.41232		
Lack-of-Fit	5	10.1346	2.02693	2.54	0.165
Pure Error	5	3.9886	0.79772		
Total	19	31.7602			

**Fig. 9** a Pareto chart represents the significant effect of three different factors, including the interactive effects on the dye removal efficiency, and b Pareto chart represents the significant effect of three different factors, including the interactive effects on the TOC removal efficiency

effect. The combined effect of temperature and salt concentration selectively induced RB5 adsorption by GIC in the presence of pH changes relative to  $pH_{pzc}$ . Initially, RB5 dye solution had a pH of 5. When the solution pH was greater than  $pH_{pzc}$ , GIC adsorbent became negatively charged, increasing its ability to adsorb more RB5 dye molecules due to GIC surface ionisation. On the GIC surfaces,  $\pi$ - $\pi$  electron donor-acceptor interactions played a significant role in the selectivity of the adsorption process. The adsorption of RB5 anionic dye on GIC surface, where an anion- $\pi$  repulsive interaction was strong due to solution pH greater than  $pH_{pzc}$ . However, the presence of  $Na^+$  ions from salt solution negated the GIC surface charges,

increasing its attraction towards anionic dye via attractive cation- $\pi$  and multivalent interactions. In addition, the adsorption process on GIC adsorbent was mainly dominated by  $\pi$ - $\pi$  and electrostatic interactions. The following represents the ANOVA analysis for the significance of interactive variables on the RB5 removal efficiency:

In addition, Table 5 represents the difference between the CCD-RSM optimised and validated results. At a typical temperature of dye wastewater at 30 °C, pH 7, and NaCl concentration of 5.50 g/L, the RB5 and TOC removal efficiencies were 14.19% and 4.71%, respectively, using CCD-RSM optimisation. These targeted responses were validated with the experimental results, which showed that

**Table 7** Comparison between optimised and non-optimised experimental results

CCD-RSM optimisation result				
Temperature (°C)	pH	Salt concentration (g/L)	TOC removal efficiency (%)	RB5 removal efficiency (%)
30	7	5.5	4.71	14.19
Experimental result for validation				
Temperature (°C)	pH	Salt concentration (g/L)	TOC removal efficiency (%)	RB5 removal efficiency (%)
30	7	5.5	4.64	13.99

RB5 and TOC removal efficiencies closely resembled the optimised values, verifying the validity of RSM optimisation (Table 7).

## Conclusion

RB5 can be removed successfully using combined adsorption and electrochemical oxidation processes. However, the optimum removal rates needed to be evaluated using CCD-RSM optimization. The results showed that pH had the most significant effect on the GIC adsorption of RB5 compared to temperature and salt concentration. Although salt concentration had a limited impact on the selectivity of GIC towards RB5, it prevented the selectivity reversal by regulating or reinforcing the balance of surface ionization of GIC, making it more conducive to RB5 adsorption. The changes in surface physicochemical properties of GIC after several cycles of electrochemical regeneration can be compensated by regulating the surface ionization of GIC, albeit additional batches of adsorption must be performed separately. In addition, the salting effect functions as a regulatory mechanism to balance or induce the surface ionisation potential of GIC adsorbent instead of directly influencing the adsorption process, whereas pH relative to the point of zero charge had a more stabilising effect on the adsorption process. On the other hand, the electrostatic interaction from the physical process helped to strengthen the adsorption process. Although GIC adsorbents were non-porous, indicating that the adsorptive capacity can be exhausted rapidly, high electrically conductive GIC adsorbents can be electrochemically regenerated to recover its active sites. The adsorption kinetics were found to follow the Elovich kinetic model, which yielded the best fitness. On the other hand, the adsorption isotherms were found to follow both SIPS and Redlich-Peterson isotherm models with significantly fewer errors than other models in accordance with error function analyses. Almost complete removal of RB5 can be achieved within 30 min at a current density of approximately 45 mA/cm<sup>2</sup>. Although the adsorptive capacity of GIC can be regenerated, further work is needed to evaluate the intermediate breakdown

products formed during the oxidation of RB5. In addition, more characterisation tests are required to examine the changes in the surface chemistry of GIC after the prolonged period of electrochemical regeneration. More methods should be explored to minimise the likelihood of particle attrition or corrosion during electrochemical treatment.

**Supplementary Information** The online version contains supplementary material available at <https://doi.org/10.1007/s13762-024-05696-4>.

**Author contributions** VG: Conceptualization, visualization, validation, investigation, formal analysis, data curation, writing—original draft. APT: Supervision, review and editing, project administration, resources.

**Funding** Open Access funding enabled and organized by CAUL and its Member Institutions. Non-applicable.

## Declarations

**Conflict of interest** The authors declare that they have no known competing financial interests or personal relationships that could have appeared to influence the work reported in this paper.

**Open Access** This article is licensed under a Creative Commons Attribution 4.0 International License, which permits use, sharing, adaptation, distribution and reproduction in any medium or format, as long as you give appropriate credit to the original author(s) and the source, provide a link to the Creative Commons licence, and indicate if changes were made. The images or other third party material in this article are included in the article's Creative Commons licence, unless indicated otherwise in a credit line to the material. If material is not included in the article's Creative Commons licence and your intended use is not permitted by statutory regulation or exceeds the permitted use, you will need to obtain permission directly from the copyright holder. To view a copy of this licence, visit <http://creativecommons.org/licenses/by/4.0/>.

## References

- Asgar HMA, Hussain SN, Sattar H, Brown NW, Roberts EPL (2014) Electrochemically synthesized GIC-based adsorbents for water treatment through adsorption and electrochemical regeneration. *J Ind Eng Chem* 20:2200–2207. <https://doi.org/10.1016/j.jiec.2013.09.051>
- Balla W, Essadki AH, Gourich B, Dassaa A, Chenik H, Azzi M (2010) Electrocoagulation/electroflotation of reactive, disperse

- and mixture dyes in an external-loop airlift reactor. *J Hazard Mater* 184:710–716. <https://doi.org/10.1016/j.jhazmat.2010.08.097>
- Chaiwichian S, Lunphut S (2021) Development of activated carbon from parawood using as adsorption sheets of organic dye in the wastewater. *Mater Today Proc* 47:3449–3453. <https://doi.org/10.1016/j.matpr.2021.03.383>
- Choi JW, Choi NC, Lee SJ, Kim DJ (2007) Novel three-stage kinetic model for aqueous benzene adsorption on activated carbon. *J Colloid Interface Sci* 314:367–372. <https://doi.org/10.1016/j.jcis.2007.05.070>
- Chu KH (2021) Revisiting the temkin isotherm: dimensional inconsistency and approximate forms. *Ind Eng Chem Res* 60:13140–13147. <https://doi.org/10.1021/acs.iecr.1c01788>
- de Fouchécour F, Larzillière V, Bouchez T, Moscoviz R (2022) Systematic and quantitative analysis of two decades of anodic wastewater treatment in bioelectrochemical reactors. *Water Res* 214:118142. <https://doi.org/10.1016/j.watres.2022.118142>
- de Vargas BG, Hashim MA, Chu KH (2023) The Sips isotherm equation: often used and sometimes misused. *Sep Sci Technol* 58:884–892. <https://doi.org/10.1080/01496395.2023.2167662>
- Droguett T, Mora-Gómez J, García-Gabaldón M, Ortega E, Mestre S, Cifuentes G, Pérez-Herranz V (2020) Electrochemical degradation of reactive black 5 using two-different reactor configuration. *Sci Rep* 10:4482. <https://doi.org/10.1038/s41598-020-61501-5>
- Elemile OO, Akpor BO, Ibitogbe EM, Afolabi YT, Ajani DO (2022) Adsorption isotherm and kinetics for the removal of nitrate from wastewater using chicken feather fiber. *Cogent Eng* 9:2043227. <https://doi.org/10.1080/23311916.2022.2043227>
- El-Kammah M, Elkhatib E, Gouveia S, Cameselle C, Aboukila E (2022) Enhanced removal of Indigo Carmine dye from textile effluent using green cost-efficient nanomaterial: adsorption, kinetics, thermodynamics and mechanisms. *Sustain Chem Pharm* 29:100753. <https://doi.org/10.1016/j.scp.2022.100753>
- Feng L, Liu J, Guo Z, Pan T, Wu J, Li X, Liu B, Zheng H (2022) Reactive black 5 dyeing wastewater treatment by electrolysis-Ce (IV) electrochemical oxidation technology: influencing factors, synergy and enhancement mechanisms. *Separ Purif Technol* 285:120314. <https://doi.org/10.1016/j.seppur.2021.120314>
- Fernandes A, Gagol M, Makoš P, Khan JA, Boczkaj G (2019) Integrated photocatalytic advanced oxidation system (TiO<sub>2</sub>/UV/O<sub>3</sub>/H<sub>2</sub>O<sub>2</sub>) for degradation of volatile organic compounds. *Separ Purif Technol* 224:1–14. <https://doi.org/10.1016/j.seppur.2019.05.012>
- Hussain SN, Asghar HMA, Sattar H, Brown NW, Roberts EPL (2015a) Free chlorine formation during electrochemical regeneration of a graphite intercalation compound adsorbent used for wastewater treatment. *J Appl Electrochem* 45:611–621. <https://doi.org/10.1007/s10800-015-0814-3>
- Hussain SN, Asghar HMA, Sattar H, Brown NW, Roberts EPL (2015b) Removal of tartrazine from water by adsorption with electrochemical regeneration. *Chem Eng Commun* 202:1280–1288. <https://doi.org/10.1080/00986445.2014.921620>
- Hussain SN, Trzcinski AP, Asghar HMA, Sattar H, Brown NW, Roberts EPL (2016) Disinfection performance of adsorption using graphite adsorbent coupled with electrochemical regeneration for various microorganisms present in water. *J Ind Eng Chem* 44:216–225. <https://doi.org/10.1016/j.jiec.2016.09.009>
- Kanneganti D, Reinersman LE, Holm RH, Smith T (2022) Estimating sewage flow rate in Jefferson County, Kentucky using machine learning for wastewater-based epidemiology applications. *Water Supply* 22:8434–8439. <https://doi.org/10.2166/ws.2022.395>
- Karimi-Jashni A, Narbaitz RM (2005) Electrochemical reactivation of granular activated carbon: effect of electrolyte mixing. *J Environ Eng* 131:443–449. [https://doi.org/10.1061/\(ASCE\)0733-9372\(2005\)131:3\(443\)](https://doi.org/10.1061/(ASCE)0733-9372(2005)131:3(443))
- Kumar D, Gupta SK (2022) Electrochemical oxidation of direct blue 86 dye using MMO coated Ti anode: modelling, kinetics and degradation pathway. *Chem Eng Process Process Intensif* 181:109127. <https://doi.org/10.1016/j.cep.2022.109127>
- Largitte L, Pasquier R (2016) A review of the kinetics adsorption models and their application to the adsorption of lead by an activated carbon. *Chem Eng Res Des* 109:495–504. <https://doi.org/10.1016/j.cherd.2016.02.006>
- Lau Y-Y, Wong Y-S, Teng T-T, Morad N, Rafatullah M, Ong S-A (2014) Coagulation-flocculation of azo dye Acid Orange 7 with green refined laterite soil. *Chem Eng J* 246:383–390. <https://doi.org/10.1016/j.cej.2014.02.100>
- Liu D, Roberts EPL, Martin AD, Holmes SM, Brown NW, Campen AK, de las Heras N (2016) Electrochemical regeneration of a graphite adsorbent loaded with Acid Violet 17 in a spouted bed reactor. *Chem Eng J* 304:1–9. <https://doi.org/10.1016/j.cej.2016.06.070>
- Ma X-Y, Fan T-T, Wang G, Li Z-H, Lin J-H, Long Y-Z (2022) High performance GO/MXene/PPS composite filtration membrane for dye wastewater treatment under harsh environmental conditions. *Compos Commun* 29:101017. <https://doi.org/10.1016/j.coco.2021.101017>
- Mansor ES, Ali H, Abdel-Karim A (2020) Efficient and reusable polyethylene oxide/polyaniline composite membrane for dye adsorption and filtration. *Colloid Interface Sci Commun* 39:100314. <https://doi.org/10.1016/j.colcom.2020.100314>
- Medeiros D, Nzediegwu C, Benally C, Messele SA, Kwak JH, Naeth MA, Ok YS, Chang SX, El-Din MG (2022) Pristine and engineered biochar for the removal of contaminants co-existing in several types of industrial wastewaters: a critical review. *Sci Total Environ* 809:151120. <https://doi.org/10.1016/j.scitotenv.2021.151120>
- Mohammed F, Roberts E, Campen A, Brown N (2012) Wastewater treatment by multi-stage batch adsorption and electrochemical regeneration. *J Electrochem Sci Eng* 2:223–236. <https://doi.org/10.5599/jese.2012.0019>
- Narbaitz R, McEwen J (2012) Electrochemical regeneration of field spent GAC from two water treatment plants. *Water Res* 46:4852–4860. <https://doi.org/10.1016/j.watres.2012.05.046>
- Nkrumah-Amoako K, Roberts EPL, Brown NW, Holmes SM (2014) The effects of anodic treatment on the surface chemistry of a graphite intercalation compound. *Electrochim Acta* 135:568–577. <https://doi.org/10.1016/j.electacta.2014.05.063>
- Noorimotlagh Z, Mirzaee SA, Martinez SS, Alavi S, Ahmadi M, Jaafarzadeh N (2019) Adsorption of textile dye in activated carbons prepared from DVD and CD wastes modified with multi-wall carbon nanotubes: equilibrium isotherms, kinetics and thermodynamic study. *Chem Eng Res Design* 141:290–301. <https://doi.org/10.1016/j.cherd.2018.11.007>
- Osorio F, Gárate Á, Russo CM (2024) The gradient test statistic for outlier detection in generalized estimating equations. *Stat Probab Lett* 209:110087. <https://doi.org/10.1016/j.spl.2024.110087>
- Purkait MK, Maiti A, DasGupta S, De S (2007) Removal of congo red using activated carbon and its regeneration. *J Hazard Mater* 145:287–295. <https://doi.org/10.1016/j.jhazmat.2006.11.021>
- Rani S, Mahajan RK (2016) Equilibrium, kinetics and thermodynamic parameters for adsorptive removal of dye Basic Blue 9 by ground nut shells and Eichhornia. *Arab J Chem* 9:S1464–S1477. <https://doi.org/10.1016/j.arabjc.2012.03.013>
- Saroyan H, Ntagiou D, Rekos K, Deliyanni E (2019) Reactive black 5 degradation on manganese oxides supported on sodium hydroxide modified graphene oxide. *Appl Sci* 9:2167. <https://doi.org/10.3390/app9102167>
- Serafin J, Dziejarski B (2023) Application of isotherms models and error functions in activated carbon CO<sub>2</sub> sorption processes.



- Microporous Mesoporous Mater 354:112513. <https://doi.org/10.1016/j.micromeso.2023.112513>
- Shahbeig H, Bagheri N, Ghorbanian S, Hallajisani A, Pourkarimi S (2013) A new adsorption isotherm model of aqueous solutions on granular activated carbon. *World J Model Simul* 9:243–254
- Song S, Fan J, He Z, Zhan L, Liu Z, Chen J, Xu X (2010) Electrochemical degradation of azo dye C.I. Reactive red 195 by anodic oxidation on Ti/SnO<sub>2</sub>-Sb/PbO<sub>2</sub> electrodes. *Electrochim Acta* 55:3606–3613. <https://doi.org/10.1016/j.electacta.2010.01.101>
- Suhan MBK, Mahtab SMT, Aziz W, Akter S, Islam MS (2021) Sudan black B dye degradation in aqueous solution by Fenton oxidation process: Kinetics and cost analysis. *Case Stud Chem Environ Eng* 4:100126. <https://doi.org/10.1016/j.cscee.2021.100126>
- Sultana M, Rownok MH, Sabrin M, Rahaman MH, Alam SMN (2022) A review on experimental chemically modified activated carbon to enhance dye and heavy metals adsorption. *Clean Eng Technol* 6:100382. <https://doi.org/10.1016/j.clet.2021.100382>
- Szygula A, Guibal E, Palacín MA, Ruiz M, Sastre AM (2009) Removal of an anionic dye (Acid Blue 92) by coagulation–flocculation using chitosan. *J Environ Manage* 90:2979–2986. <https://doi.org/10.1016/j.jenvman.2009.04.002>
- Tekin D (2014) Photocatalytic degradation of textile dyestuffs using TiO<sub>2</sub> nanotubes prepared by sonoelectrochemical method. *Appl Surface Sci* 318:132–136. <https://doi.org/10.1016/j.apsusc.2014.02.018>
- Tzabar N, ter Brake HJM (2016) Adsorption isotherms and Sips models of nitrogen, methane, ethane, and propane on commercial activated carbons and polyvinylidene chloride. *Adsorption* 22:901–914. <https://doi.org/10.1007/s10450-016-9794-9>
- Wu F-C, Tseng R-L, Juang R-S (2009) Characteristics of Elovich equation used for the analysis of adsorption kinetics in dye-chitosan systems. *Chem Eng J* 150:366–373. <https://doi.org/10.1016/j.cej.2009.01.014>
- Wu F-C, Liu B-L, Wu K-T, Tseng R-L (2010) A new linear form analysis of Redlich–Peterson isotherm equation for the adsorptions of dyes. *Chem Eng J* 162:21–27. <https://doi.org/10.1016/j.cej.2010.03.006>
- Xing X, Tang J, Yao S, Chen H, Zheng T, Wu J (2023) Electrochemical regeneration of granular activated carbon saturated by p-nitrophenol in BDD anode system. *Process Saf Environ Protect* 170:207–214. <https://doi.org/10.1016/j.psep.2022.11.082>

